

1
2 DR GRÁINNE DONOHUE (Orcid ID : 0000-0003-3828-0872)

3 MR. BRIAN JOSEPH KEOGH (Orcid ID : 0000-0001-6349-486X)

4
5
6 Article type : Research Article

7
8
9
10 **Mapping Lung Ventilation through Stress**
11 **Maps Derived from Biomechanical Models**
12 **of the Lung**

13 **Guillaume Cazoulat^{1*}, James M Balter², Martha M Matuszak²,**
14 **Shruti Jolly², Dawn Owen², and Kristy K Brock¹**

15 ¹ Department of Imaging Physics, The University of Texas MD Anderson Cancer
16 Center, Houston, TX

17 ² Department of Radiation Oncology, University of Michigan, Ann Arbor, MI

18 *Corresponding author: gcazoulat@mdanderson.org - MD Anderson Cancer Center,
19 Imaging Physics - Research, 1515 Holcombe Blvd., Unit 1902, Houston, TX 77030-
20 4009

21 **Abstract**

22
23 **Purpose:** Most existing CT-ventilation imaging techniques are based on deformable
24 image registration (DIR) of different respiratory phases of a 4DCT scan of the lung,
25 followed by the quantification of local breathing-induced changes in Hounsfield Units
26 (HU) or volume. To date, only moderate correlations have been reported between
27 these CT-ventilation metrics and standard ventilation imaging modalities for adaptive
28 lung radiation therapy. This study evaluates the use of stress maps derived from
29 biomechanical model-based DIR as an alternative CT-ventilation metric.

This is the author manuscript accepted for publication and has undergone full peer review but has not been through the copyediting, typesetting, pagination and proofreading process, which may lead to differences between this version and the [Version of Record](#). Please cite this article as [doi: 10.1002/MP.14643](https://doi.org/10.1002/MP.14643)

This article is protected by copyright. All rights reserved

30 **Materials and Methods:** Six patients treated for lung cancer with conventional
31 radiation therapy were retrospectively analyzed. For each patient, a 4DCT scan and
32 Tc-99m SPECT-V image acquired for treatment planning were collected.
33 Biomechanical model-based DIR was applied between the inhale and exhale phase of
34 the 4DCT scans and stress maps were calculated. The voxel-wise correlation between
35 the reference SPECT-V image and map of the maximum principal stress was
36 measured with a Spearman correlation coefficient. The overlap between high (above
37 the 75th percentile) and low (below the 25th percentile) functioning volumes extracted
38 from the reference SPECT-V and the stress maps were measured with Dice similarity
39 coefficients (DSC). The results were compared to those obtained when using two
40 classical CT-ventilation metrics: the change in HU and Jacobian determinant.

41 **Results:** The mean Spearman correlation coefficients were: 0.37 ± 18 and 0.39 ± 13 and
42 0.59 ± 0.13 considering the changes in HU, Jacobian and maximum principal stress,
43 respectively. The corresponding mean DSC coefficients were 0.38 ± 0.09 , 0.37 ± 0.07
44 and 0.52 ± 0.07 for the high ventilation function volumes and 0.48 ± 0.13 , 0.44 ± 0.09 and
45 0.52 ± 0.07 for the low ventilation function volumes.

46 **Conclusion:** For presenting a significantly stronger and more consistent correlation
47 with standard SPECT-V images than previously proposed CT-ventilation metrics,
48 stress maps derived with the proposed method appear to be a promising tool for
49 incorporation into functional lung avoidance strategies.

50

51 **Running title:** Stress map-based CT-ventilation imaging

52 **Keywords:** lung cancer, biomechanics, CT-ventilation imaging

53 1. Introduction

54 Management of lung cancer includes radiation therapy for the majority of patients.¹
55 A common side-effect of lung radiotherapy, and a limiting factor for dose escalation trials, is
56 radiation induced pneumonitis.²⁻⁶ To reduce the risk of toxicity, functional lung avoidance
57 techniques have been proposed, consisting of taking into account the spatial heterogeneity of
58 the lung function at planning into the optimization process of the dose distribution.^{7,8} The
59 definition of functional volumes for planning has typically relied on the acquisition of
60 ventilation/perfusion single photon emission computed tomography (SPECT) scan in
61 addition to the standard Computed Tomography (CT) scans acquired for treatment
62 planning.⁹

63 Previous studies have suggested that the lung ventilation functional distribution
64 could be derived from the planning CT scan alone, which would enable functional lung
65 avoidance without increasing the burden for the patient and financial cost of the treatment

66 protocol. This concept, named CT-ventilation imaging and used in three clinical US trials
67 for functional lung avoidance (NCT02528942, NCT02308709, NCT0284356), mainly
68 relies on the calculation of two metrics after deformable image registration (DIR) between
69 different temporal phases of 4D CT scans typically acquired to assess the movement of
70 tumors and/or other organs to assist target definition for patients treated while breathing
71 freely. The first approach consisted of estimating the ventilation at each corresponding voxel
72 in the lungs as a function of change in Hounsfield Units (HU).¹⁰ A second approach focused
73 on estimating the local ventilation by calculating the local volume change given by the
74 determinant of the Jacobian of the displacement vector field (DVF).¹¹ Other studies have
75 since reported correlation measures between CT-ventilation maps, derived by these or other
76 methods, and reference lung function maps extracted from images such as SPECT
77 ventilation/perfusion,¹²⁻¹⁵ contrast-enhanced Xenon CT for sheep,^{16,17} hyperpolarized
78 magnetic resonance (MR)¹⁸ or positron emission tomography (PET) using ⁶⁸GaCl₃-labeled
79 pseudogas (“Galligas”).¹⁹ These studies have demonstrated a correlation between the CT-
80 ventilation maps and reference images when considering the contribution of sub-volumes of
81 the lung to the total ventilation function. However, in the studies that reported a voxel-wise
82 correlation between the CT-ventilation maps and reference ventilation images, a weak and
83 highly variable correlation was found for SPECT images^{14,20} and at best was qualified as
84 moderate for PET Galligas images¹⁹.

85 Among existing DIR strategies for CT scans of the lung, a method based on
86 biomechanical modeling has previously been demonstrated to provide accurate displacement
87 vector fields (DVF), especially in registering the exhale to the inhale phase of 4DCT scans.²¹
88 This finite-element model (FEM)-based method (Morfeus) has the additional advantage,
89 compared to traditional DIR algorithms, of allowing the definition of heterogeneous elastic
90 properties inside the lung while controlling local deformation based on image features, in
91 this case the lung and vasculature segmentations. It has been demonstrated that this method
92 provides an accurate estimation of the DVF, and therefore the strain distribution in the lung.
93 Assuming that the local ventilation function is proportional to the local air-induced volume
94 change, which can be measured directly by the strain given by DIR, and to the local density
95 of normal lung tissue (which might be related to the elasticity), the stress, defined as the
96 product of strain and elasticity, appears as a natural metric for this ventilation function. In
97 this paper, we propose to expand the biomechanical model-based DIR method to calculate
98 mechanical stress maps and evaluate their correlation with reference ventilation imaging.

99 Recently, the VAMPIRE Challenge was conducted, aiming to quantify the
100 variability in proposed CT-ventilation maps based on different DIR methods and CT-
101 ventilation metric as well as their correlation with three different reference ventilation image

102 modalities: Xenon CT for sheep, DTPA-SPECT and Galligas 4DPET/CT for humans.²²
103 Considering stress maps as the CT-ventilation metric as an alternative to other proposed
104 metrics yielded a substantially higher correlation with the reference imaging for the human
105 datasets. This paper describes the method to generate the stress maps and provides further
106 evaluation of the correlation with SPECT-V data from six additional patients not included in
107 the VAMPIRE Challenge.

108
109

110 **2. Materials and methods**

111 *2.1. Patient data*

112

113 Six lung cancer patients who underwent SPECT-V scans as part of treatment on an
114 IRB-approved adaptive radiation therapy protocol were retrospectively analyzed for this
115 study. Each patient had a 4DCT scan for planning, reconstructed using 10 bins with axial
116 spatial resolution ranging from 0.93 to 1.18 mm and consistent slice spacing of 3 mm. The
117 inhale and exhale phases were selected by visually assessing which phases presented with
118 the minimum and maximum lung inflation levels. Contours of the left and right lungs were
119 manually delineated on both phases in the treatment planning system (Eclipse, Varian
120 Medical Systems, Palo Alto, California, USA). For all patients, a ventilation Tc-99m SPECT
121 (SPECT-V) scan of resolution 0.9x0.9x2 mm was acquired prior to treatment and used for
122 analysis.

123
124

125 *2.2. Stress maps computation*

126

127 The workflow of the biomechanical model-based deformable registration method
128 (Morfeus) used for the lung is represented Figure 1 and has previously been described in
129 detail.²¹ Briefly, it consists first of generating a tetrahedral mesh of the lung and body from
130 the contours of the reference fixed image, in this case the inhale phase of the 4DCT. A
131 surface projection algorithm was then used between the lung surfaces defined on the two
132 images, based on the computation of distance maps from the lung contours followed by
133 application of DIR with a variant of the Demons algorithm. The displacements estimated by
134 the Demons algorithm were used to define boundary conditions in the FEM. Instead of
135 applying displacements directly on the lung surface nodes, the displacements were applied
136 on the chest cavity nodes. Thanks to the definition of a frictionless contact surface between

137 the lung and chest wall, this approach allowed to simulate the physiological lung sliding and
138 to limit the impact of a possible inaccurate surface projection.²³ In parallel, vessels were
139 automatically segmented in the two images and non-rigidly registered to define boundary
140 conditions on their centerline. A numerical simulation of the displacement of all nodes of the
141 mesh was finally performed using the finite-element analysis software Optistruct (Altair
142 Engineering, Troy, MI).

143 The introduction of heterogeneous elastic properties in this workflow was
144 demonstrated to have a negligible impact on the resulting DVF.²⁴ However, in order to
145 accurately calculate the stress distribution, or the local resistance of the lung tissue to the
146 deformation imposed by the boundary conditions, variations in elastic properties of the lung
147 must be defined. A wide range of elastic properties were considered in previous work on
148 finite-element modeling of the lung with a linear elastic model, with a Poisson's ratio
149 ranging from 0.1 to 0.49 and a Young's modulus ranging from 0.1 to 7.8 kPa.²⁵⁻²⁸ In this
150 study, based on these orders of magnitude, the elements' compressibility was assumed
151 constant with a Poisson's ratio set to 0.4 as in the previously proposed Morfeus workflow
152 for DIR and variable Young's moduli (E) were assigned to different regions of the lung
153 ranging from 1 kPa for the definition of air to a maximum of 20 kPa for the definition of the
154 stiffest lung tissues such as fibrosis.

155 The assignment of different elastic properties in the FEM and the generation of
156 stress maps are illustrated in Figure 2. To estimate the Young's modulus spatial distribution,
157 a linear relationship was assumed with the density of lung tissue given by the HU in the
158 inhale CT scan. Voxels with HU below -950 were considered as air only and those with HU
159 above -200 as the stiffest tissue. The stiffness in all other voxels was assumed linearly
160 proportional to the corresponding HU. Each tetrahedral element of the lung was assigned a
161 Young's modulus based on the density at the tetrahedron centroid location in the inhale CT.
162 Since the tetrahedral mesh resolution (5 mm) was much coarser than the image, the inhale
163 CT scan was first smoothed with a Gaussian filter of radius 6 mm to ensure a smooth
164 distribution of the stiffness in the mesh. To obtain a single scalar value at the centroid
165 coordinates \mathbf{c}_k of each tetrahedron k of the mesh, the maximum principal stress σ_{k_1} , defined
166 as the maximum eigenvalue of the Cauchy stress tensor $\boldsymbol{\sigma}_k$, was calculated by the finite-
167 element analysis software Optistruct (Altair Engineering). The scattered σ_{k_1} distribution was
168 then resampled on the grid of the reference image to generate a stress map V_{Stress} directly
169 comparable to a reference ventilation function map.

170

171

172 **2.3. SPECT-V and stress maps similarity analysis**

173

174 The SPECT-V was aligned with the average CT generated from the planning 4DCT
175 in the TPS Eclipse as performed for treatment planning. The same comparison was
176 performed between the generated and reference ventilation images as in many CT-
177 ventilation imaging studies, in particular the VAMPIRE challenge.²²

178 First, the Spearman correlation coefficient was calculated between the generated
179 stress maps and reference ventilation images in a mask defined by the contours of the lung
180 in the exhale image. This coefficient measures the strength of the monotonicity between the
181 two-paired distributions.

182 Second, in order to compare the identification of high and low functioning volumes
183 in the lung, thresholds were applied to the stress maps and SPECT-based ventilation maps
184 based on the individual patient's map. For each patient's individual stress map and SPECT
185 ventilation map, the low functioning volume included all lung voxels below the 25th
186 percentile of the patient's specific map distribution and the high functioning volume all lung
187 voxels above the 75th percentile. Dice similarity coefficients (DSC) were calculated between
188 the high and low functional volumes extracted from the stress maps and the reference
189 SPECT-V images. The patient-specific determination of the high and low functioning
190 volumes of the lung is acceptable as the ventilation maps are used to assess relative lung
191 function on individual patients (as opposed to the whole patient population).

192

193 2.4. Comparison with other methods

194

195 The similarity results obtained with the analysis of the V_{Stress} maps were compared
196 to those obtained when considering the two other mainly used CT-ventilation metrics: the
197 local volume change and local change in air density. The local volume change was
198 measured by the Jacobian determinant J of the inverse of the DVF calculated from Morfeus,
199 so that a local tissue expansion yielded $J > 1$ and a local contraction $J < 1$ as in [11]. The
200 corresponding CT-ventilation map was noted V_{Jac} . The CT-ventilation map based on change
201 in air density, noted V_{HU} , was also calculated using the inverse of the DVF from Morfeus
202 and following the equation¹⁹:

203

$$V_{HU}(\mathbf{x}) = \frac{I_{ex}(\mathbf{x}) - I_{in}(\mathbf{x} + \mathbf{u})}{I_{in}(\mathbf{x} + \mathbf{u}) + 1000},$$

204 with I_{ex} and I_{in} respectively the exhale and inhale images and the displacement vector \mathbf{u} at
205 the corresponding voxel coordinates \mathbf{x} . For comparison of the results with previous studies,
206 the V_{Jac} and V_{HU} maps were smoothed with a median filter of width 3x3x3 voxels.²²

207 Statistical differences between the mean Spearman correlation coefficients and
208 mean DSCs obtained with the different CT-ventilation methods were assessed with two-
209 tailed paired t-tests.

210

211 **3. Results**

212 *3.1. Spearman correlation coefficients*

213

214 Figure 3 shows the breathing motion magnitude for the six patients with a color
215 overlay between coronal slices of the inhale and exhale phases of the 4DCT scans. For each
216 patient, the following were also represented on the same coronal slice: the SPECT-V image,
217 the computed stress map and a scatter plot of their relationship. For visualization purposes,
218 the SPECT-V and stress images were normalized for each patient by linearly rescaling the 0-
219 90th percentiles between 0 and 1 and by setting the visualization window/level to 1/0.5.

220 Various forms of ventilation function distributions were observed. Patient 1 did not
221 present any particular ventilation defect, with the entire lung demonstrating breathing-
222 induced motion. On the reference SPECT-V image, areas of high ventilation function could
223 be observed near the direct exit of the main airways and the signal globally decreased with
224 the distance to these areas of high ventilation. The stress map computed for this patient
225 presented a similar pattern due to the higher stiffness defined around the main vasculature.
226 The SPECT images for Patients 2 and 3 presented low ventilation function in the upper lobe
227 of their right and left lung, respectively. These defects, which were likely due to an
228 obstruction of the airflow by the tumor, could also be observed on the generated stress maps
229 resulting from the low volume change (e.g. low strain) calculated in this area. Patient 4 was
230 the case presenting the lowest correlation between SPECT-V and stress. It appeared that the
231 imaging aerosol did not enter the right lung at the time of the SPECT acquisition whereas the
232 4DCT scan seemed to exhibit ventilation-induced volume change of the right middle and
233 inferior lobes. However, the correlation for the left lobe alone appeared high. The highest
234 Spearman correlation coefficients, above 0.7, were obtained for Patient 5 and 6 who both
235 presented large regions with poor ventilation function. For Patient 5, the defect corresponded
236 to the presence of emphysema in the upper part of the lungs while for Patient 6, the airways
237 were obstructed preventing the air to enter the middle and upper lobe of the right lung.

238 Figure 4 reports the Spearman correlation coefficients measured between the three
239 different CT-ventilation calculations and the SPECT-V intensity distribution. With a mean
240 Spearman coefficient of 0.59 ± 0.13 , the correlation between the stress maps and reference
241 imaging was significantly higher ($p < 0.05$) than when considering the Jacobian (0.39 ± 0.13) or

242 changes in HU (0.37 ± 18). The stress map provided the highest correlation with the SPECT-
243 V ventilation map for all patients except Patient 4. We hypothesize that this difference could
244 be due to an actual variation of the ventilation function between the time of the SPECT and
245 planning 4DCT acquisitions or a limitation of the aerosol to propagate to that area of the
246 lung, despite normal lung ventilation, that appeared to be depicted on the 4DCT.

247

248

249 3.2. Dice similarity coefficients (DSC)

250

251 Table 1 reports the DSCs obtained between the high and low ventilation function
252 volumes derived from the CT-ventilation maps and those extracted from corresponding
253 SPECT-V images. For all six patients, the DSC of the high function volume was higher
254 when derived from the stress map than from the Jacobian or change in HU, and the mean
255 was significantly higher ($p < 0.01$). For the low function volumes, the stress maps yielded the
256 highest DSC for all but 2 patients (4 and 6). The DSC values for the low function volumes
257 obtained with the stress maps were significantly higher than with the Jacobian ($p < 0.01$) but
258 not higher than those obtained with the change in HU ($p = 0.12$), an effect that was mostly
259 due to the differences observed for Patient 4.

260

261 Patients 5 and 6, who presented the highest Spearman correlation
262 coefficients between the stress map and SPECT-V, also presented the highest DSC between
263 corresponding functional volumes. Figure 5 represents the low and high function volumes
264 for those two patients who presented two different kinds of defects. Patient 5 exhibited
265 emphysema in the superior parts of both lungs. Because of the resulting low HU values, the
266 biomechanical model assigned a low elasticity in this area, leading to low stress values.
267 Patient 6 exhibited relatively normal tissues across the whole lung but the disease prevented
268 the aeration of the middle and superior lobes of the right lung, leading to the absence of
269 motion estimated by the biomechanical DIR and so to low stress values. The highest
270 ventilation function areas given by the SPECT-V images were found for these two patients
271 in the rest of the lung where the vasculature density was high. As a consequence of defining
272 these areas as stiffer in the biomechanical model, the stress map showed consistent high
273 values.

274

275

276 **4. Discussion**

277 In terms of correlation with SPECT-V images, the method outperformed other
278 methods based on the computation of the Jacobian determinant or changes in HU alone. The
279 stress maps presented the highest correlation with SPECT for all of the six patients analyzed
280 but one, for whom the HU-change method performed better. For the methods based on the
281 Jacobian or changes in HU, other DIR algorithms may potentially yield to a higher
282 correlation but the Spearman coefficients obtained in this study, with mean values of
283 0.39 ± 13 and 0.37 ± 18 respectively, were similar with the highest coefficients previously
284 reported. A case scenario for which the Jacobian determinant alone was likely to present a
285 poor correlation with reference ventilation imaging is when bullae or emphysema were
286 present in the lung as it has been illustrated previously²⁹ and in this study. Volume
287 expansions were indeed still occurring in these areas following inspiration despite the
288 absence of lung function. The inverse of the DVF was used for the determinant of the
289 Jacobian and no constraint in this algorithm ensured inverse consistency in the DVF which
290 may be a limitation in this calculation. The interpretation of the performance of the HU
291 changes-based method is more challenging. One drawback of this HU-based method could
292 be a higher sensitivity to image artifacts, which are common with 4DCT imaging and can
293 lead locally to a completely wrong estimation of the intensity. By using only contours of the
294 lung and autosegmentation of the vasculature to estimate the deformation, Morfeus is
295 probably less sensitive to these motion artifacts than global intensity-based DIR methods,
296 but the estimated CT-ventilation metrics could still be impacted.

297 The V_{Jac} and V_{HU} maps computed in this study were implemented to serve as a
298 baseline as they correspond to the most commonly used CT-ventilation imaging metrics.
299 Variants or combinations of these metrics may lead to a stronger correlation. However, the
300 results reported in this paper are consistent with those recently reported for other datasets
301 and other ventilation imaging modalities in the context of the VAMPIRE Challenge.²² The
302 proposed algorithm performed the best for the two validation datasets of human subjects,
303 one of 20 PET-Galligas and one of 11 DTPA-SPECT, with mean Spearman correlation
304 coefficients of 0.53 ± 0.10 and 0.49 ± 16 , respectively.

305 Uncertainties with the proposed biomechanical model-based method may come
306 from the assumption of a linear relationship between the local density of the tissue in the CT
307 scans and the stiffness. The choice of the Young's modulus range was empirical. However,
308 since variations in the Young's modulus had little impact on the strain estimation and since
309 ventilation maps are intended to provide relative and not absolute values of the ventilation
310 function, the choice of this range does not matter as long as it ensures a linear relationship

311 between the stress and strain. To ensure a smooth distribution of the elasticity in the FEM,
312 the Young's moduli assigned to the mesh nodes were based on a Gaussian smoothing of the
313 CT image. Without this type of filtering, mesh nodes located close to but outside of vessels
314 could be assigned low Young's moduli and the model could underestimate the local
315 stiffness. The optimal radius of the Gaussian filter is directly related to the resolution of the
316 FEM, with finer meshes which capture more anatomical information requiring smaller
317 image smoothing. These two parameters were chosen empirically in this study and their
318 optimal value will be optimized in future work based on a larger cohort of patients.

319 ■ No consensus exists regarding the minimum required Spearman correlation
320 coefficient to indicate that a CT-ventilation map is considered a good surrogate to the
321 reference ventilation image. In a study comparing radiotherapy plans optimized using either
322 SPECT or CT-ventilation maps for functional lung avoidance, the authors found that when
323 the Spearman coefficient between the two ventilation maps was on the order of 0.4, a
324 reasonable agreement was observed between the final functional lung sparing planned dose
325 distributions.³⁰ For all patients in this study with the exception of Patient 4, the Spearman
326 correlation coefficient between the stress map and SPECT-V image was consistently greater
327 than 0.5, suggesting the proposed method could serve as a good surrogate for SPECT-V for
328 treatment planning purposes. Achieving a higher correlation might be possible, especially
329 considering recent advances in deep learning techniques, but without necessarily being more
330 clinically relevant for current models of functional sparing in treatment planning. Existing
331 ventilation mapping methods are indeed known to be associated with uncertainties and
332 artifacts. Especially, while it was not the case for the six patients analyzed in this study,
333 SPECT-V image quality commonly suffers from clumping of the aerosol in the airways.³¹
334 The mechanistic approach proposed in this study may provide a more reliable mapping of
335 the actual ventilation function.

336

337 **5. Conclusion**

338 This paper describes an original approach to generate lung ventilation function images
339 through stress maps derived from biomechanical model-based DIR. The generated
340 ventilation maps presented a significantly stronger and more consistent correlation with
341 standard SPECT-V images than previously proposed CT-ventilation metrics did. We believe
342 this approach is a very promising tool for incorporation in functional lung avoidance
343 strategies.

344

345 **Acknowledgments**

346 This work was funded in part by NIH P01CA059827.

347

348 **Conflicts of interest**

349 Kristy Brock received funding from RaySearch Laboratories AB through a Co-Development
350 and Collaboration Agreement. Kristy Brock has a licensing agreement with RaySearch
351 Laboratories AB. Martha Matuszak received research and consulting funding from Varian
352 Medical Systems. Shruti Jolly is a consultant for Varian Medical Systems and AstraZeneca.

353

354 **References**

- 355 1. Tyldesley S, Boyd C, Schulze K, Walker H, Mackillop WJ. Estimating the need for
356 radiotherapy for lung cancer: an evidence-based, epidemiologic approach.
357 *International Journal of Radiation Oncology* Biology* Physics*. 2001;49(4):973-
358 985.
- 359 2. Sura S, Gupta V, Yorke E, Jackson A, Amols H, Rosenzweig KE. Intensity-
360 modulated radiation therapy (IMRT) for inoperable non-small cell lung cancer: The
361 Memorial Sloan-Kettering Cancer Center (MSKCC) experience. *Radiotherapy and
362 Oncology*. 2008;87(1):17-23.
- 363 3. Yamashita H, Takahashi W, Haga A, Nakagawa K. Radiation pneumonitis after
364 stereotactic radiation therapy for lung cancer. *World journal of radiology*.
365 2014;6(9):708-715.
- 366 4. Marks LB, Bentzen SM, Deasy JO, et al. Radiation Dose–Volume Effects in the
367 Lung. *International Journal of Radiation Oncology* Biology* Physics*. 2010;76(3,
368 Supplement):S70-S76.
- 369 5. Yom SS, Liao Z, Liu HH, et al. Initial Evaluation of Treatment-Related
370 Pneumonitis in Advanced-Stage Non–Small-Cell Lung Cancer Patients Treated
371 With Concurrent Chemotherapy and Intensity-Modulated Radiotherapy.
372 *International Journal of Radiation Oncology* Biology* Physics*. 2007;68(1):94-102.
- 373 6. Rodrigues G, Lock M, D'Souza D, Yu E, Van Dyk J. Prediction of radiation
374 pneumonitis by dose–volume histogram parameters in lung cancer—a systematic
375 review. *Radiotherapy and Oncology*. 2004;71(2):127-138.
- 376 7. Marks LB, Spencer DP, Sherouse GW, et al. The role of three dimensional
377 functional lung imaging in radiation treatment planning: The functional dose-

- 378 volume histogram. *International Journal of Radiation Oncology*Biology*Physics*.
379 1995;33(1):65-75.
- 380 8. Siva S, Thomas R, Callahan J, et al. High-resolution pulmonary ventilation and
381 perfusion PET/CT allows for functionally adapted intensity modulated radiotherapy
382 in lung cancer. *Radiotherapy and Oncology*. 2015;115(2):157-162.
- 383 9. Eslick EM, Stevens MJ, Bailey DL. SPECT V/Q in Lung Cancer Radiotherapy
384 Planning. *Seminars in Nuclear Medicine*. 2019;49(1):31-36.
- 385 10. Guerrero T, Sanders K, Noyola-Martinez J, et al. Quantification of regional
386 ventilation from treatment planning CT. *International Journal of Radiation
387 Oncology*Biology*Physics*. 2005;62(3):630-634.
- 388 11. Reinhardt JM, Ding K, Cao K, Christensen GE, Hoffman EA, Bodas SV.
389 Registration-based estimates of local lung tissue expansion compared to xenon CT
390 measures of specific ventilation. *Medical image analysis*. 2008;12(6):752-763.
- 391 12. Castillo R, Castillo E, Martinez J, Guerrero T. Ventilation from four-dimensional
392 computed tomography: density versus Jacobian methods. *Physics in medicine and
393 biology*. 2010;55(16):4661-4685.
- 394 13. Castillo R, Castillo E, McCurdy M, et al. Spatial correspondence of 4D CT
395 ventilation and SPECT pulmonary perfusion defects in patients with malignant
396 airway stenosis. *Physics in medicine and biology*. 2012;57(7):1855-1871.
- 397 14. Hegi-Johnson F, Keall P, Barber J, Bui C, Kipritidis J. Evaluating the accuracy of
398 4D-CT ventilation imaging: First comparison with Technegas SPECT ventilation.
399 *Med Phys*. 2017;44(8):4045-4055.
- 400 15. Yamamoto T, Kabus S, Lorenz C, et al. Pulmonary ventilation imaging based on 4-
401 dimensional computed tomography: comparison with pulmonary function tests and
402 SPECT ventilation images. *International Journal of Radiation Oncology* Biology*
403 Physics*. 2014;90(2):414-422.
- 404 16. Fuld MK, Easley RB, Saba OI, et al. CT-measured regional specific volume change
405 reflects regional ventilation in supine sheep. *Journal of applied physiology
406 (Bethesda, Md : 1985)*. 2008;104(4):1177-1184.
- 407 17. Ding K, Cao K, Fuld MK, et al. Comparison of image registration based measures
408 of regional lung ventilation from dynamic spiral CT with Xe-CT. *Medical physics*.
409 2012;39(8):5084-5098.
- 410 18. Mathew L, Wheatley A, Castillo R, et al. Hyperpolarized ³He Magnetic Resonance
411 Imaging: Comparison with Four-dimensional X-ray Computed Tomography
412 Imaging in Lung Cancer. *Academic Radiology*. 2012;19(12):1546-1553.

- 413 19. Kipritidis J, Siva S, Hofman MS, Callahan J, Hicks RJ, Keall PJ. Validating and
414 improving CT ventilation imaging by correlating with ventilation 4D-PET/CT
415 using 68Ga-labeled nanoparticles. *Med Phys*. 2014;41(1):011910.
- 416 20. Yamamoto T, Kabus S, von Berg J, et al. Evaluation of four-dimensional (4D)
417 computed tomography (CT) pulmonary ventilation imaging by comparison with
418 single photon emission computed tomography (SPECT) scans for a lung cancer
419 patient. Paper presented at: Proceedings of the Third International Workshop on
420 Pulmonary Image Analysis2010.
- 421 21. ■ Cazoulat G, Owen D, Matuszak MM, Balter JM, Brock KK. Biomechanical
422 deformable image registration of longitudinal lung CT images using vessel
423 information. *Physics in Medicine & Biology*. 2016;61(13):4826.
- 424 22. Kipritidis J, Tahir BA, Cazoulat G, et al. The VAMPIRE challenge: A multi-
425 institutional validation study of CT ventilation imaging. *Med Phys*.
426 2019;46(3):1198-1217.
- 427 23. ■ Al-Mayah A, Moseley J, Velec M, Brock KK. Sliding characteristic and material
428 compressibility of human lung: Parametric study and verification. *Medical physics*.
429 2009;36(10):4625-4633.
- 430 24. Al-Mayah A, Moseley J, Velec M, Hunter S, Brock K. Deformable image
431 registration of heterogeneous human lung incorporating the bronchial tree. *Medical
432 physics*. 2010;37(9):4560-4571.
- 433 25. Sundaram TA, Gee JC. Towards a model of lung biomechanics: pulmonary
434 kinematics via registration of serial lung images. *Medical image analysis*.
435 2005;9(6):524-537.
- 436 26. Zhang T, Orton NP, Mackie TR, Paliwal BR. A novel boundary condition using
437 contact elements for finite element based deformable image registration. *Medical
438 physics*. 2004;31(9):2412-2415.
- 439 27. Al-Mayah A, Moseley J, Brock K. Contact surface and material nonlinearity
440 modeling of human lungs. *Physics in Medicine & Biology*. 2007;53(1):305.
- 441 28. Villard P-F, Beuve M, Shariat B, Baudet V, Jaillet F. Simulation of lung behaviour
442 with finite elements: Influence of bio-mechanical parameters. Paper presented at:
443 Third International Conference on Medical Information Visualisation--BioMedical
444 Visualisation2005.
- 445 29. Kipritidis J, Hofman MS, Siva S, et al. Estimating lung ventilation directly from 4D
446 CT Hounsfield unit values. *Medical Physics*. 2016;43(1):33-43.

- 447 30. Kida S, Bal M, Kabus S, et al. CT ventilation functional image-based IMRT
448 treatment plans are comparable to SPECT ventilation functional image-based plans.
449 *Radiotherapy and Oncology*. 2016;118(3):521-527.
- 450 31. Schembri GP, Roach PJ, Bailey DL, Freeman L. Artifacts and Anatomical Variants
451 Affecting Ventilation and Perfusion Lung Imaging. *Seminars in nuclear medicine*.
452 2015;45(5):373-391.

453
454
455 *Figure 1. Morfeus workflow for the deformable image registration between the inhale and*
456 *exhale phases of a 4DCT scan.*

457 *Figure 2. Expansion of the Morfeus method workflow described in Figure 1 for the*
458 *generation of stress maps.*

459 *Figure 3. Illustration of the breathing magnitude between the inhale and exhale phases of*
460 *the 4DCT and of the correlation between the reference SPECT-V images and*
461 *computationally generated stress maps.*

462 *Figure 4. Spearman correlation coefficients between each CT-ventilation metric and the*
463 *reference SPECT-V for the six patients.*

464 *Figure 5. Representation for the two patients presenting the highest correlation between*
465 *stress maps and reference SPECT-V images of the low and high function volumes obtained*
466 *by thresholding. The plain red and green area represent respectively the low and high*
467 *function volumes derived from the SPECT-V. The blue and orange contours represent the*
468 *same volumes but derived from the stress maps.*

Table 1. Dice similarity coefficients between ventilation function volumes from CT-ventilation maps and reference SPECT-V images.

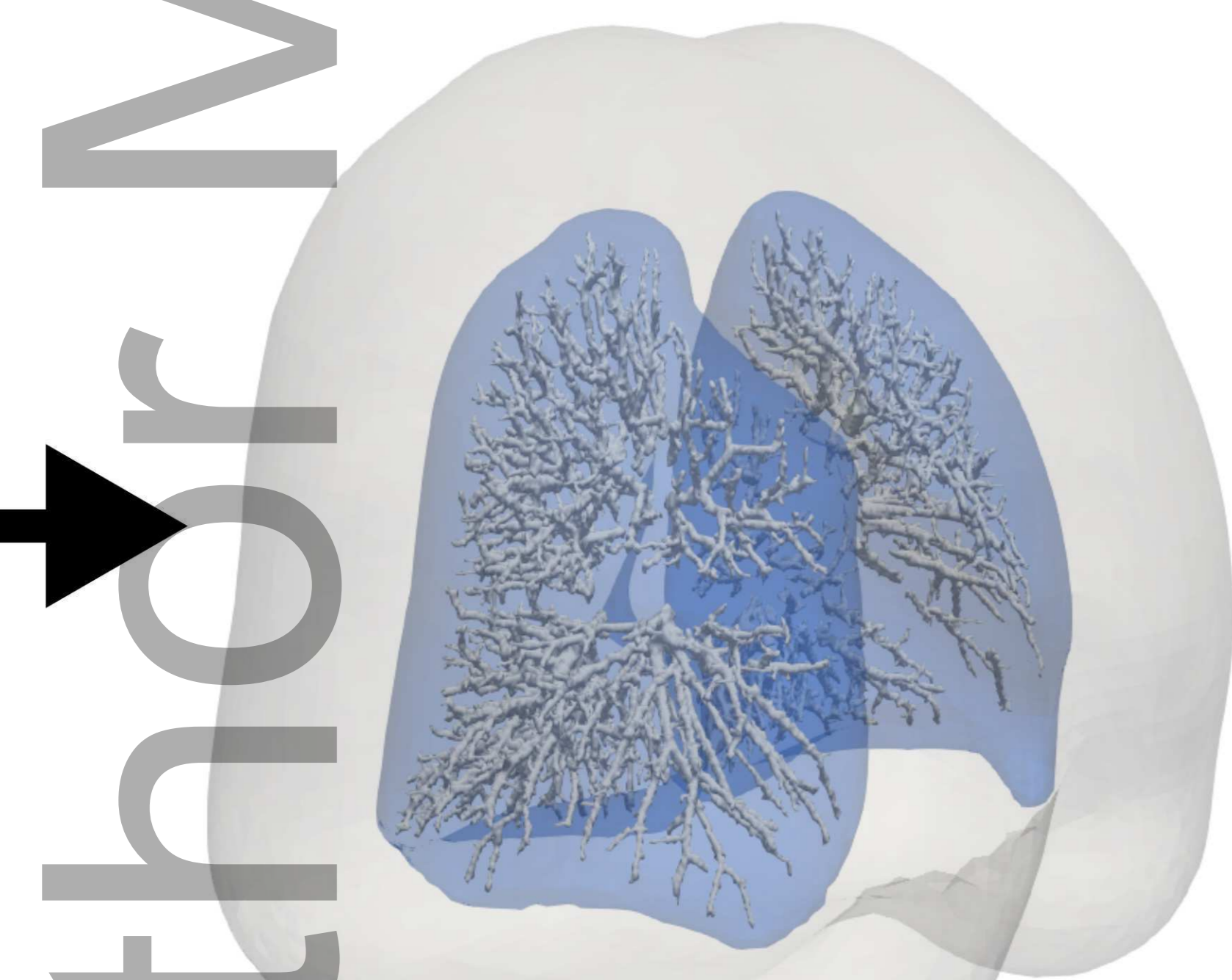
	Low function volume DSC			High function volume DSC		
	Stress	Jacobian	HU	Stress	Jacobian	HU
Patient1	0.55	0.49	0.48	0.52	0.43	0.40
Patient2	0.52	0.31	0.33	0.46	0.24	0.29
Patient3	0.65	0.49	0.47	0.42	0.35	0.28
Patient4	0.39	0.36	0.46	0.52	0.36	0.50
Patient5	0.66	0.43	0.41	0.57	0.44	0.45
Patient6	0.69	0.55	0.72	0.60	0.40	0.34
Mean	0.58	0.44	0.48	0.52	0.37	0.38
STD	0.11	0.09	0.13	0.07	0.07	0.09



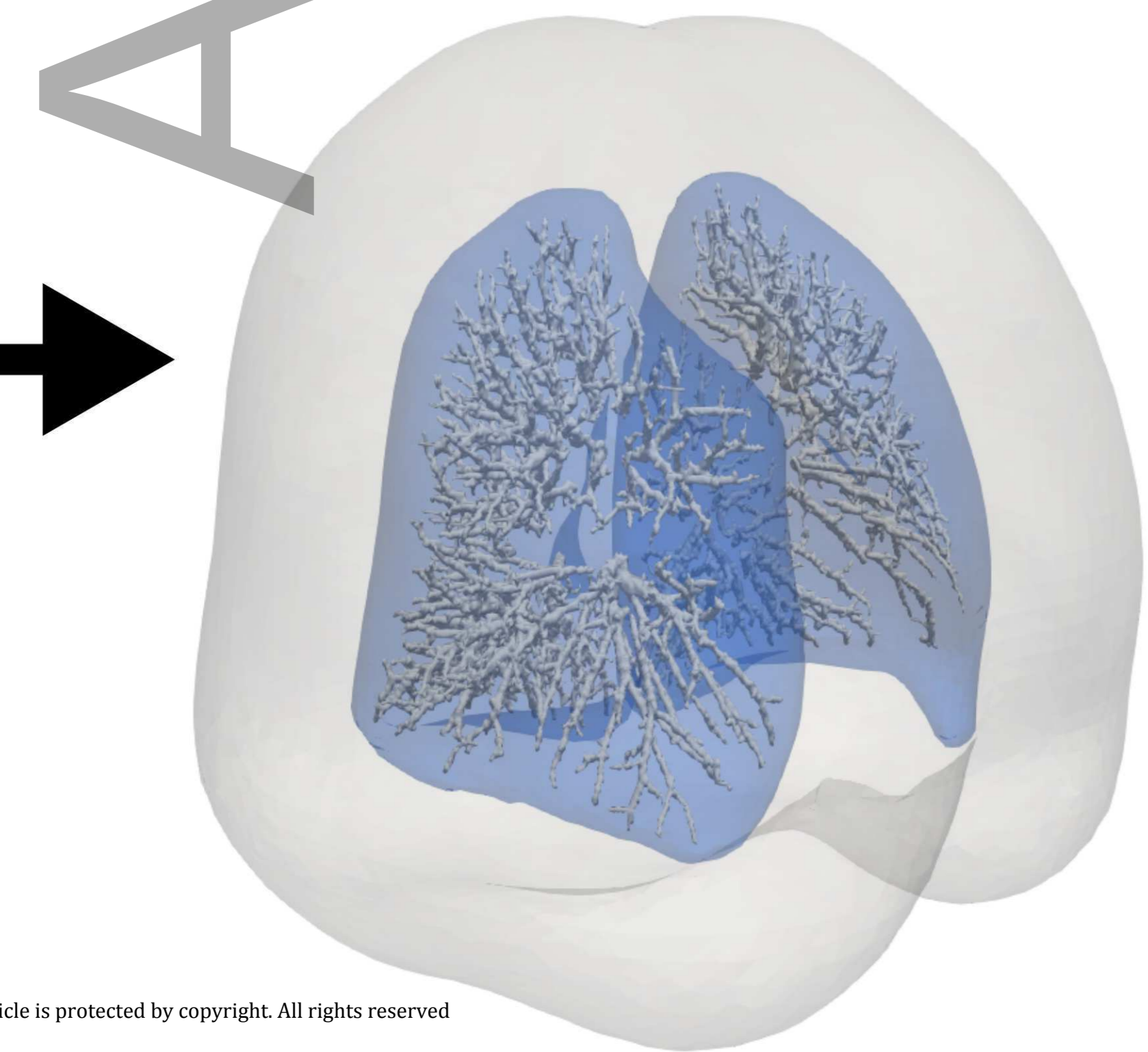
Inhale phase



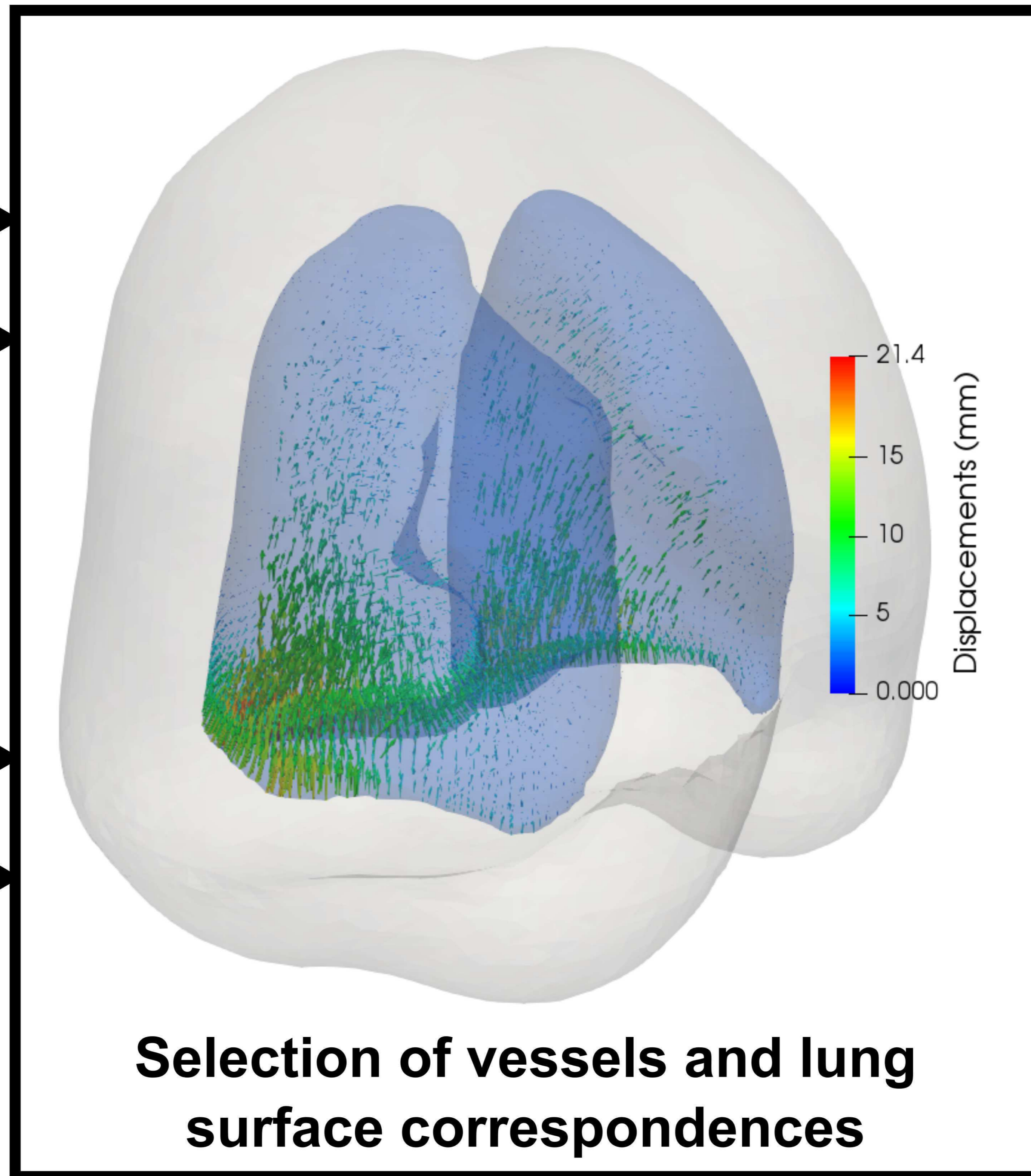
Exhale phase



Vessels segmentation

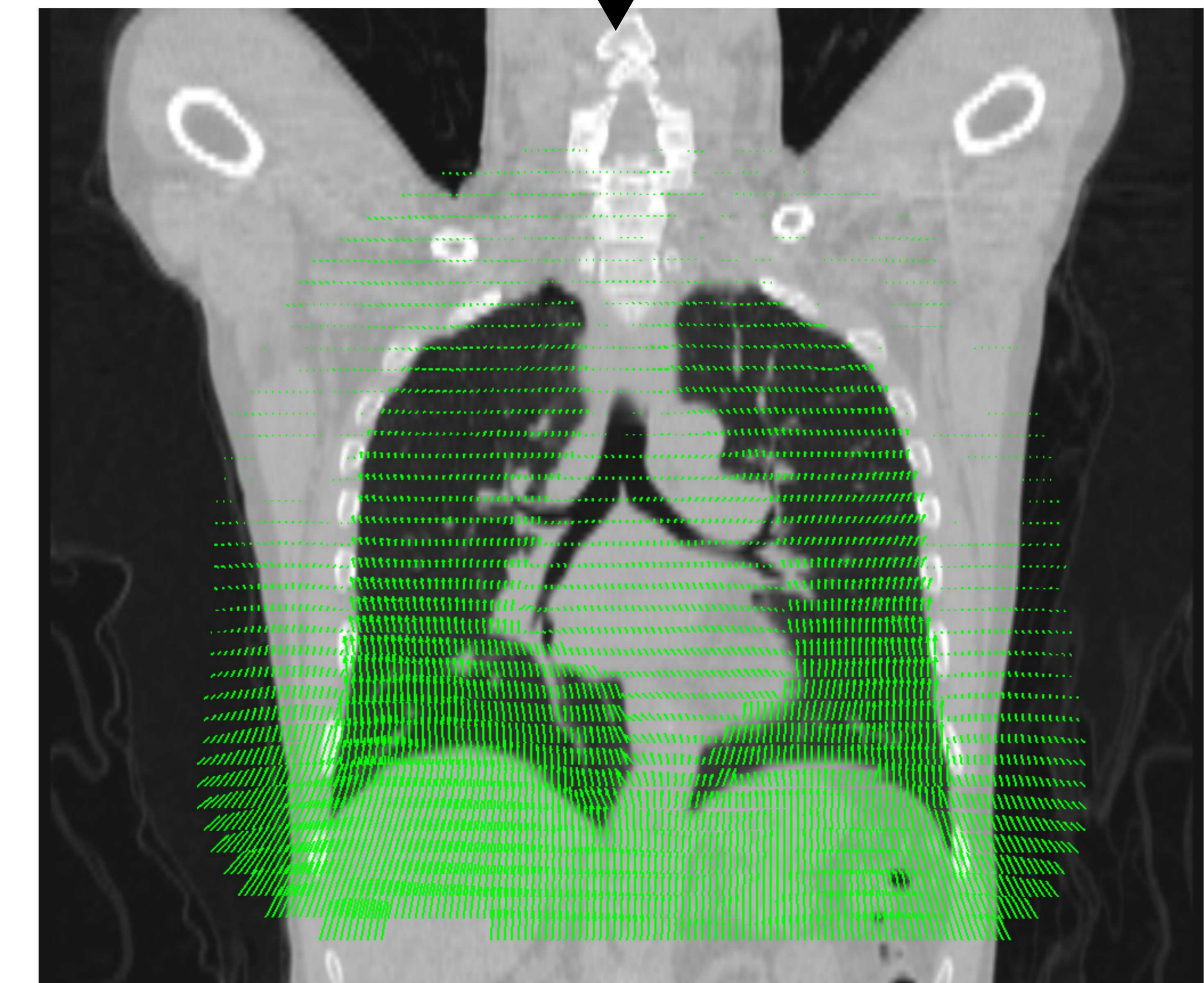


Linear elastic finite-element modeling
Lungs + Body + Contact surface



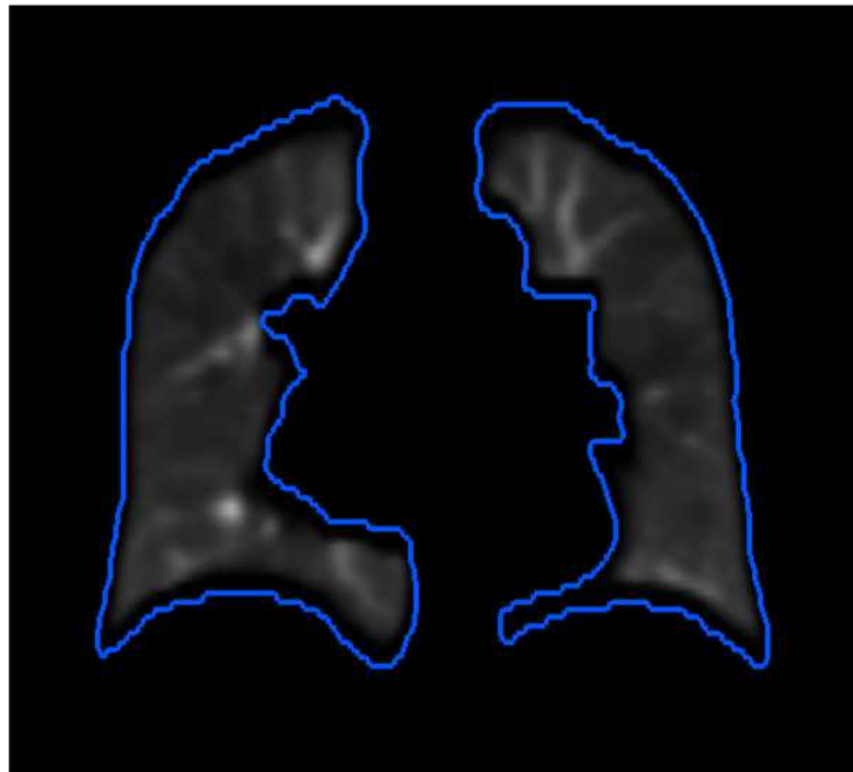
Selection of vessels and lung
surface correspondences

Finite-element
analysis

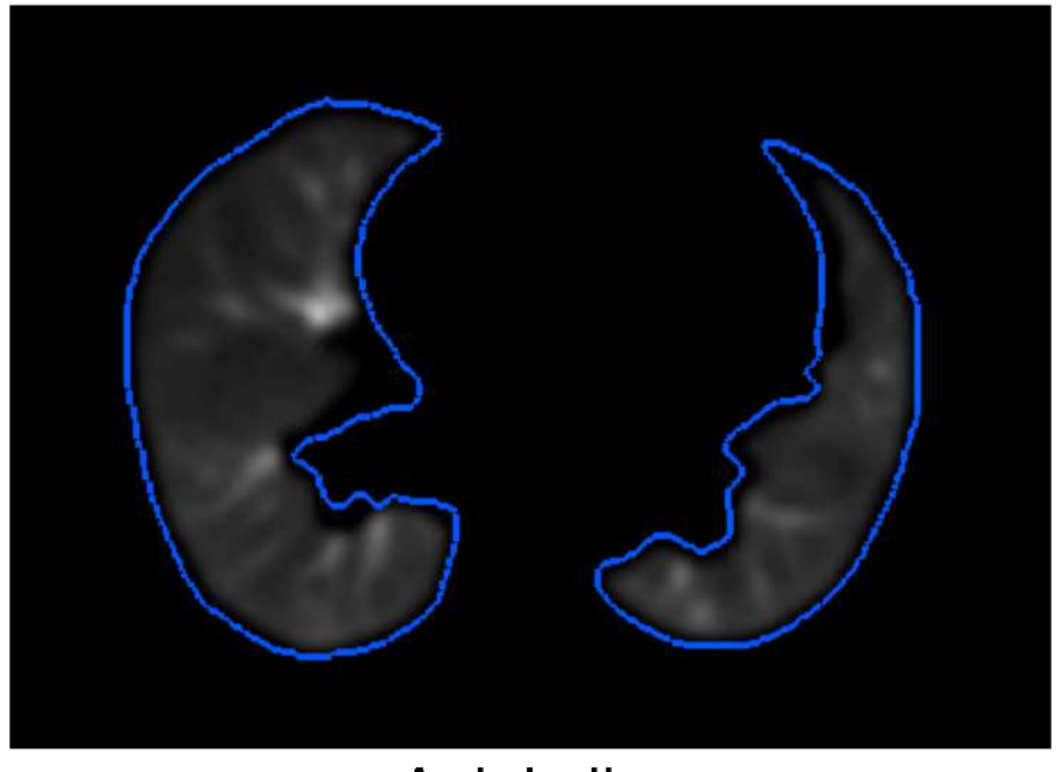


Displacement vector field

Gaussian smoothing of the lung Hounsfield Units



Coronal slice

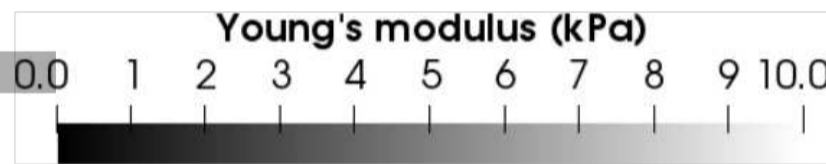
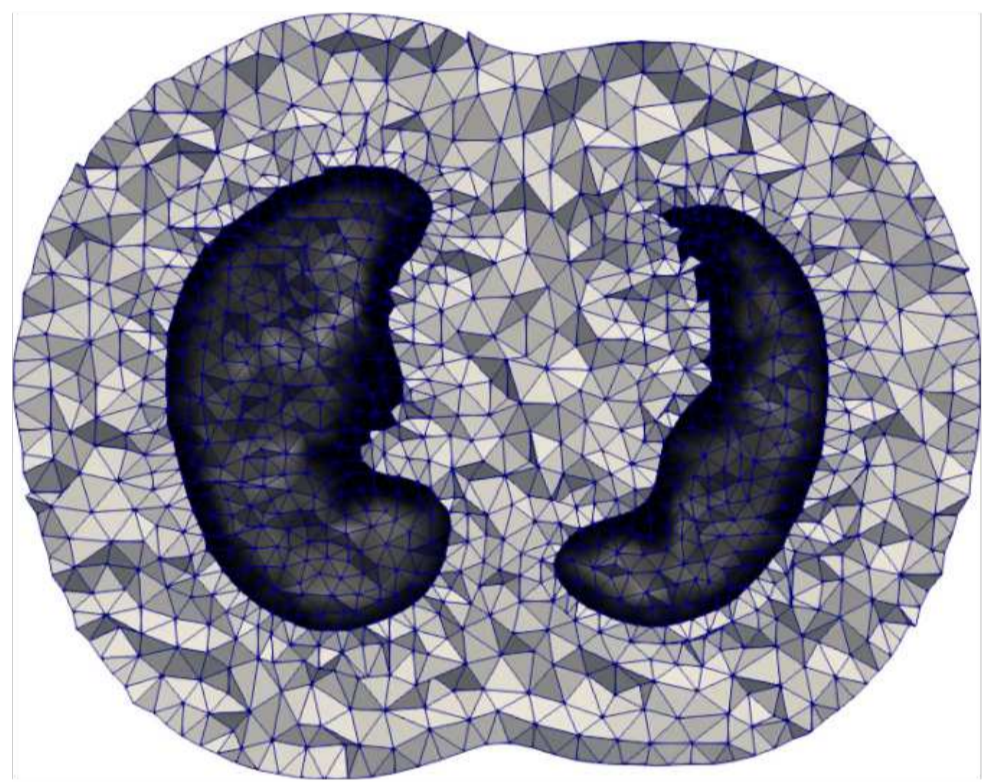
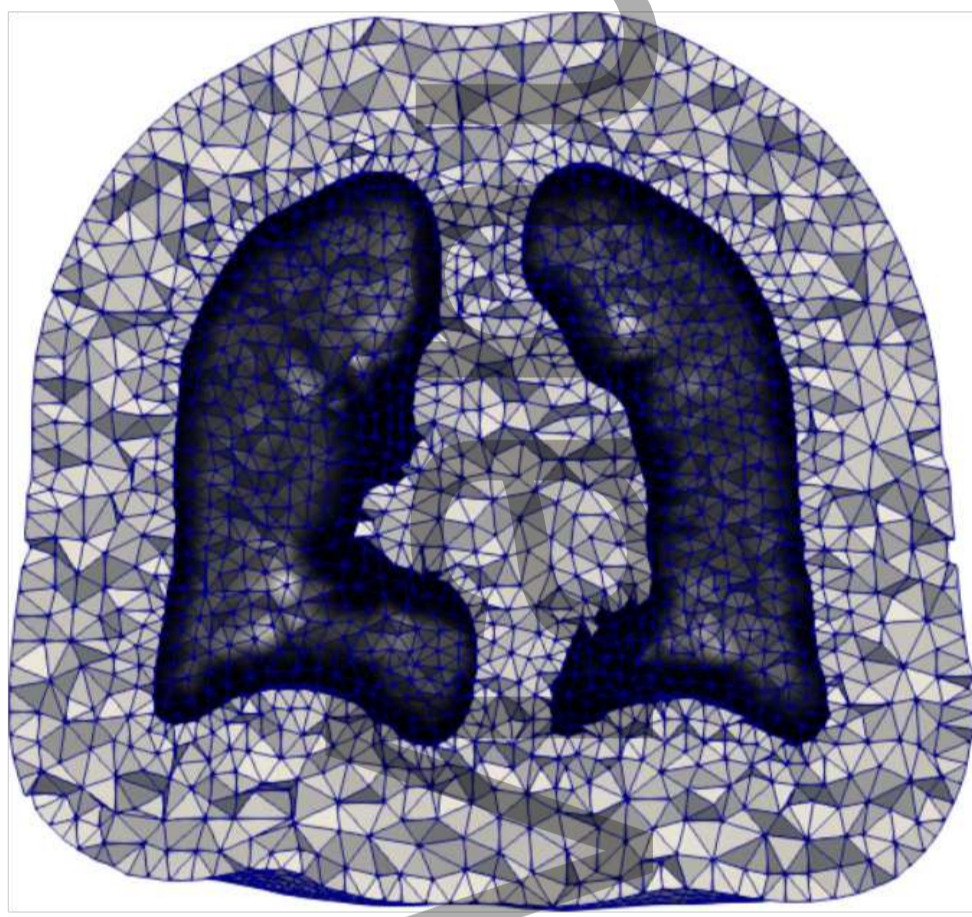


Axial slice

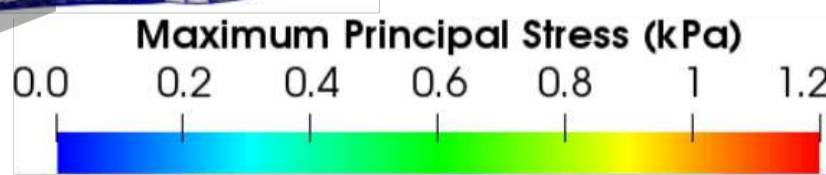
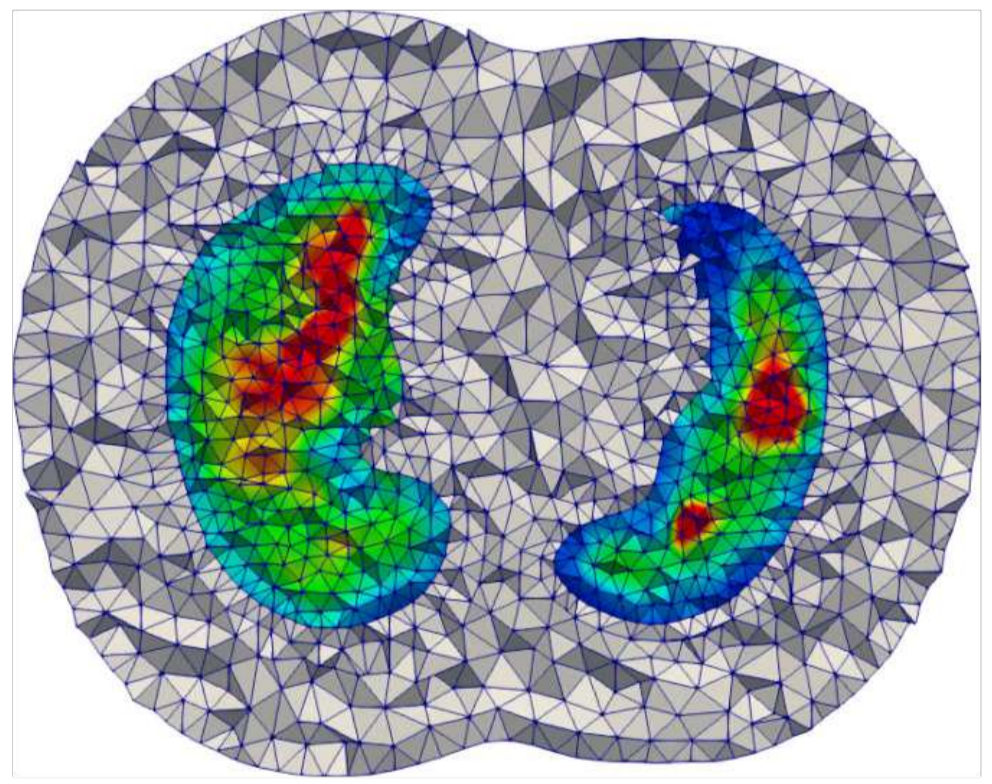
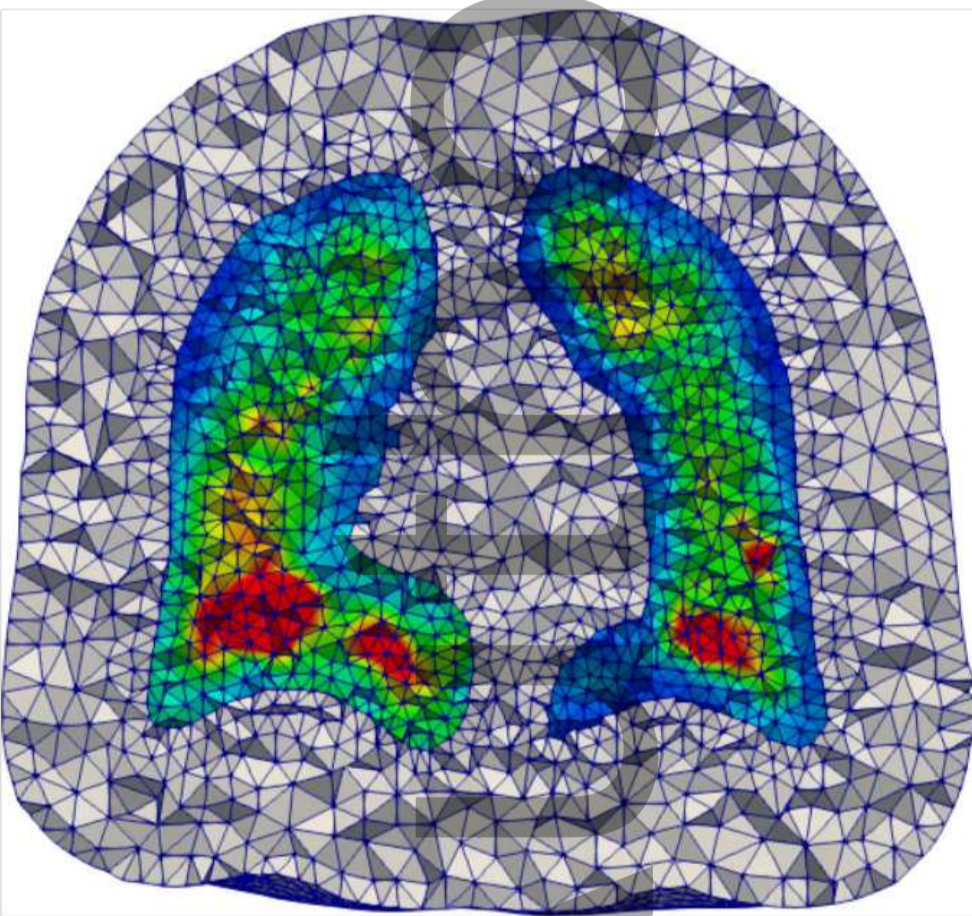
Conversion of Hounsfield Units to Young's modulus



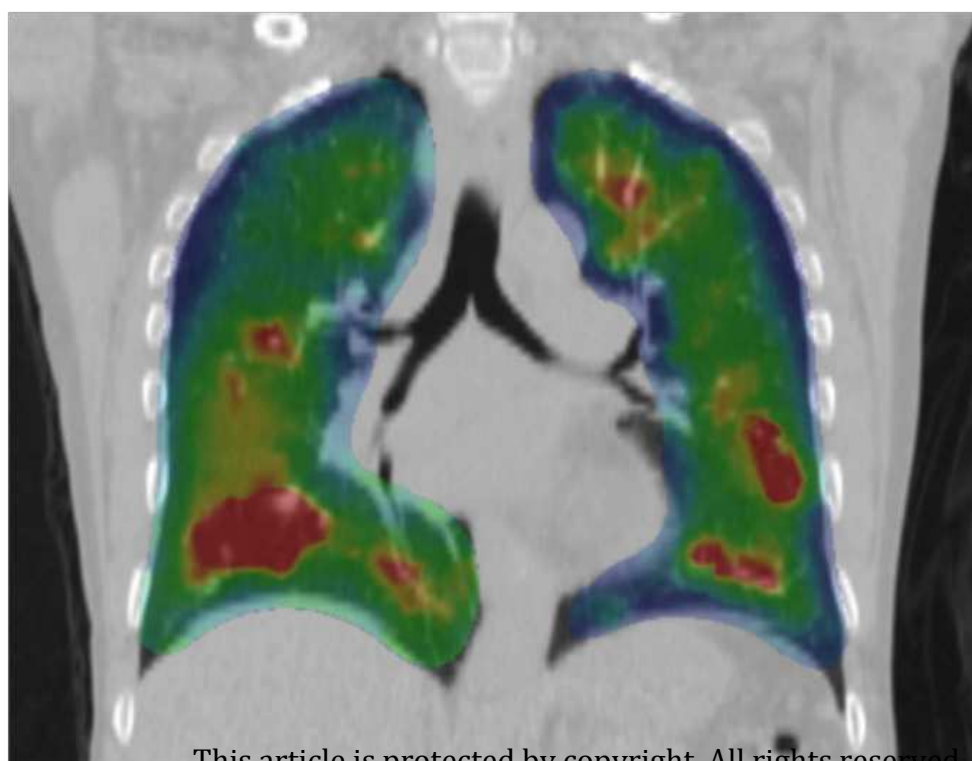
Finite-element modeling Assignment of heterogeneous Young's modulus



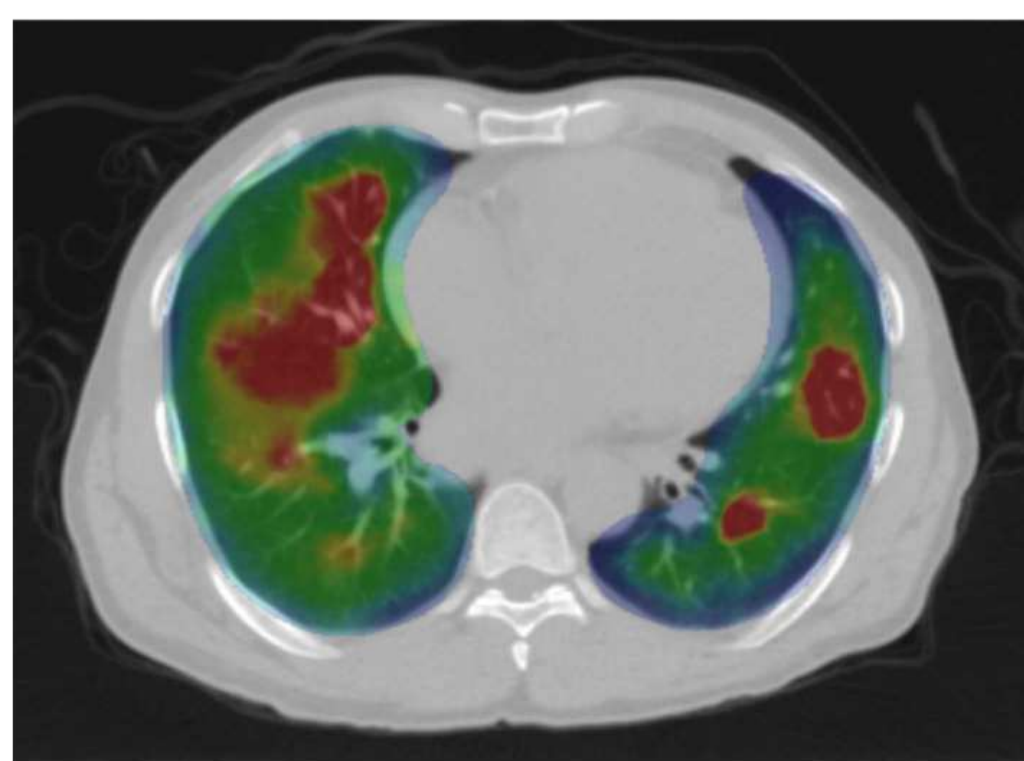
Finite-element analysis - Stress computation



Resampling on the CT scan grid



Coronal slice



Axial slice

Overlay Inhale/Exhale

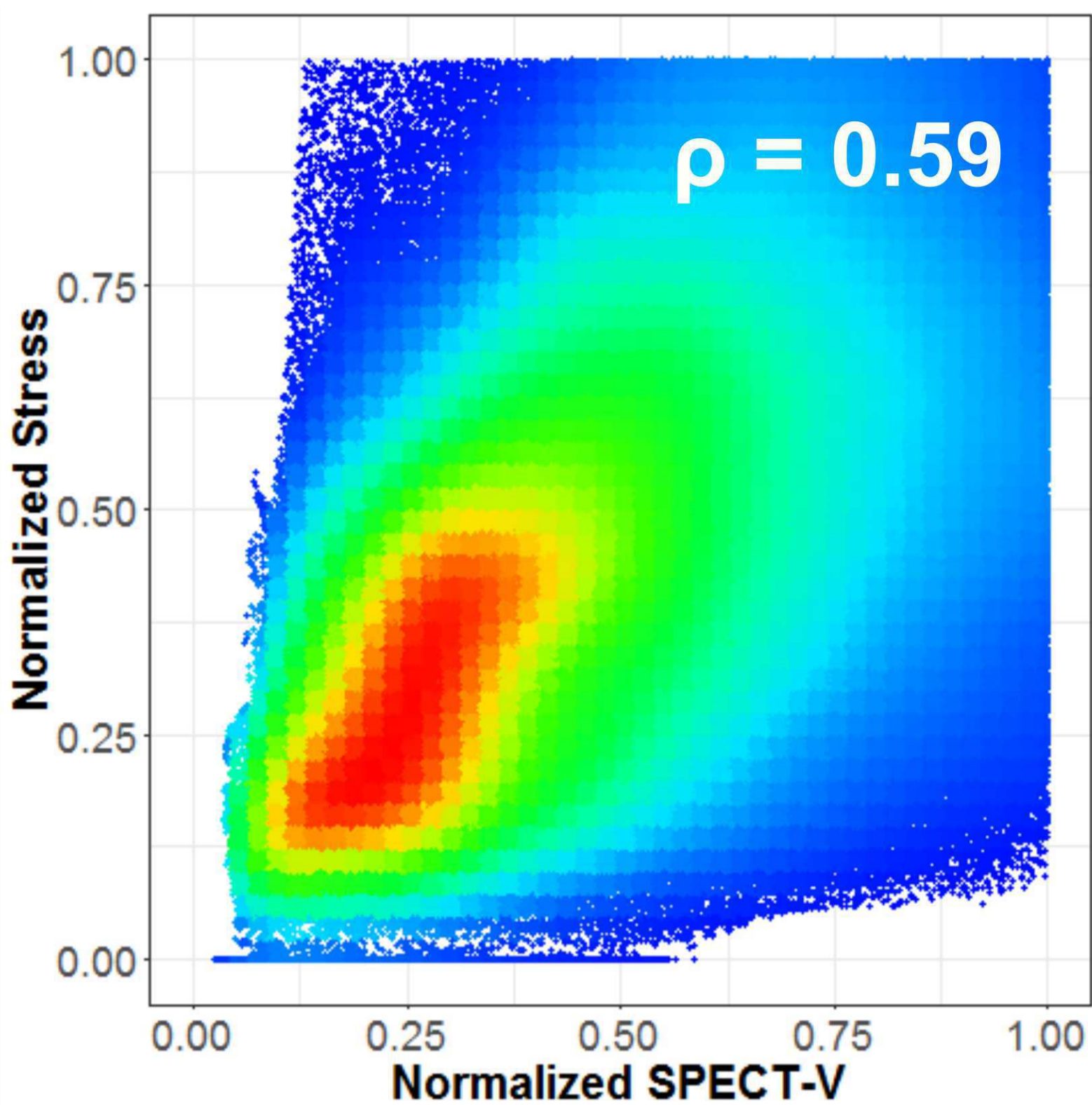
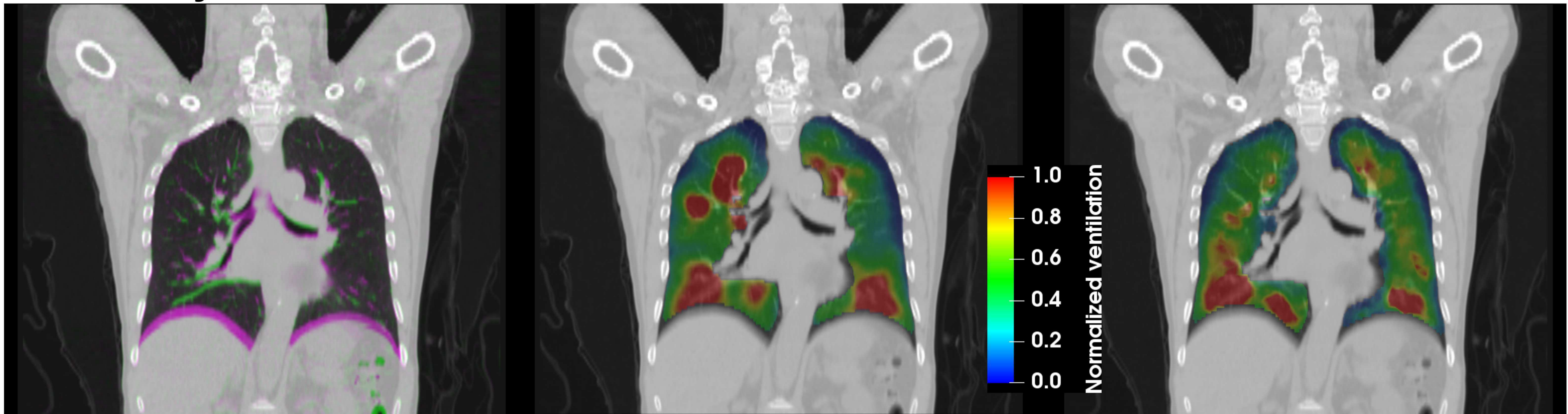
SPECT-V

mp_14643_0.pdf

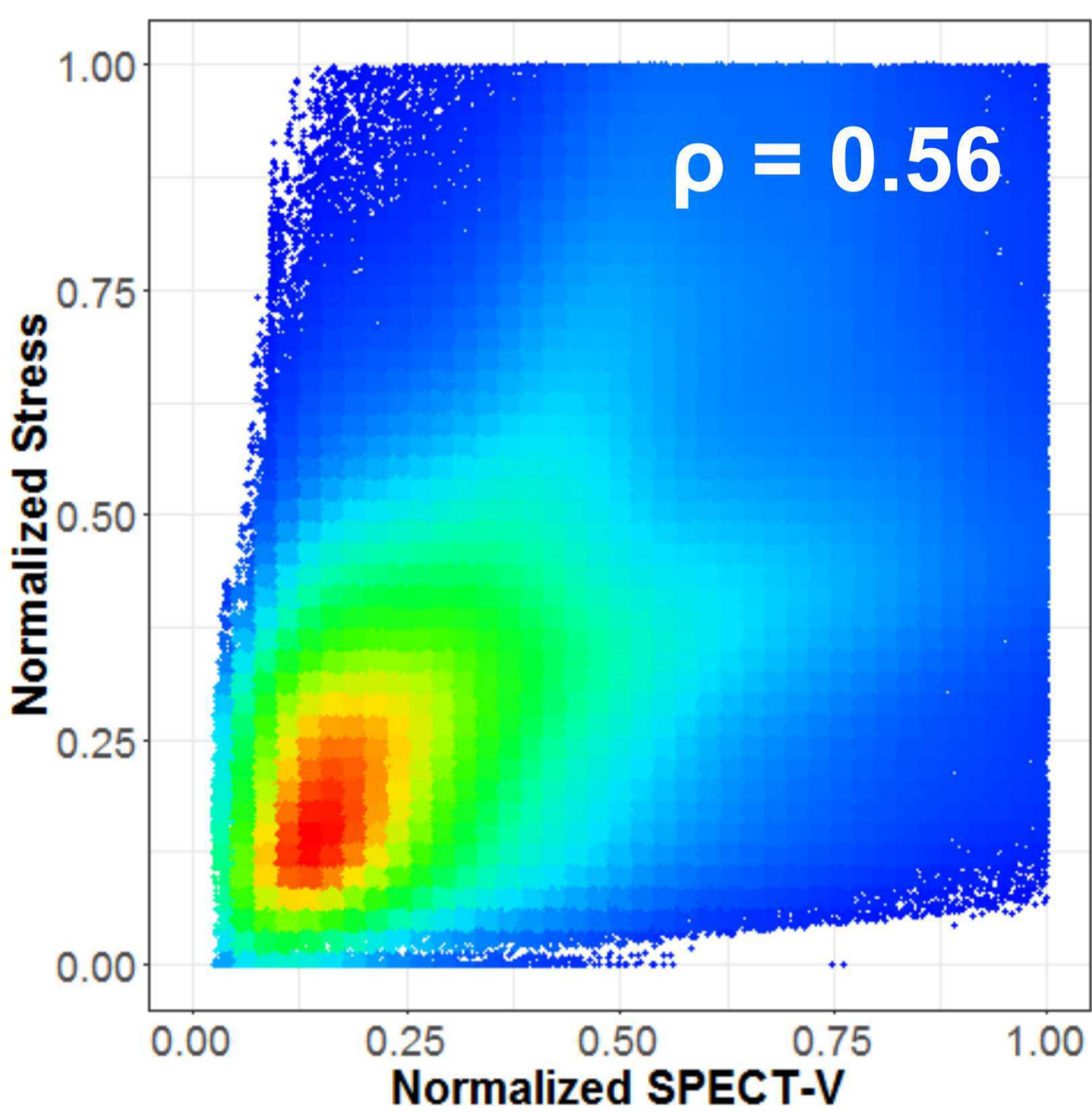
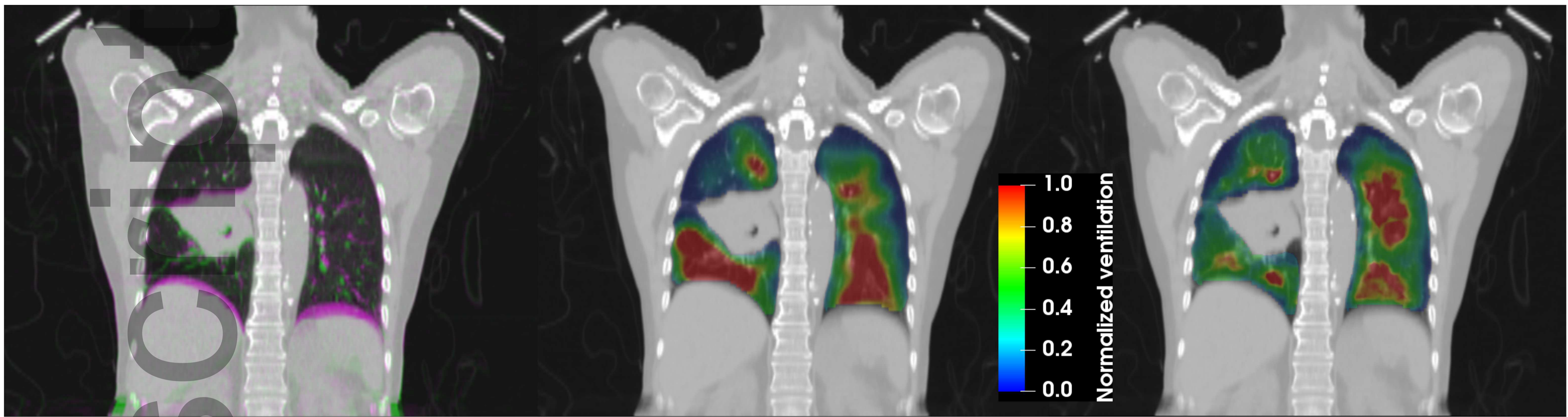
Stress

Correlation

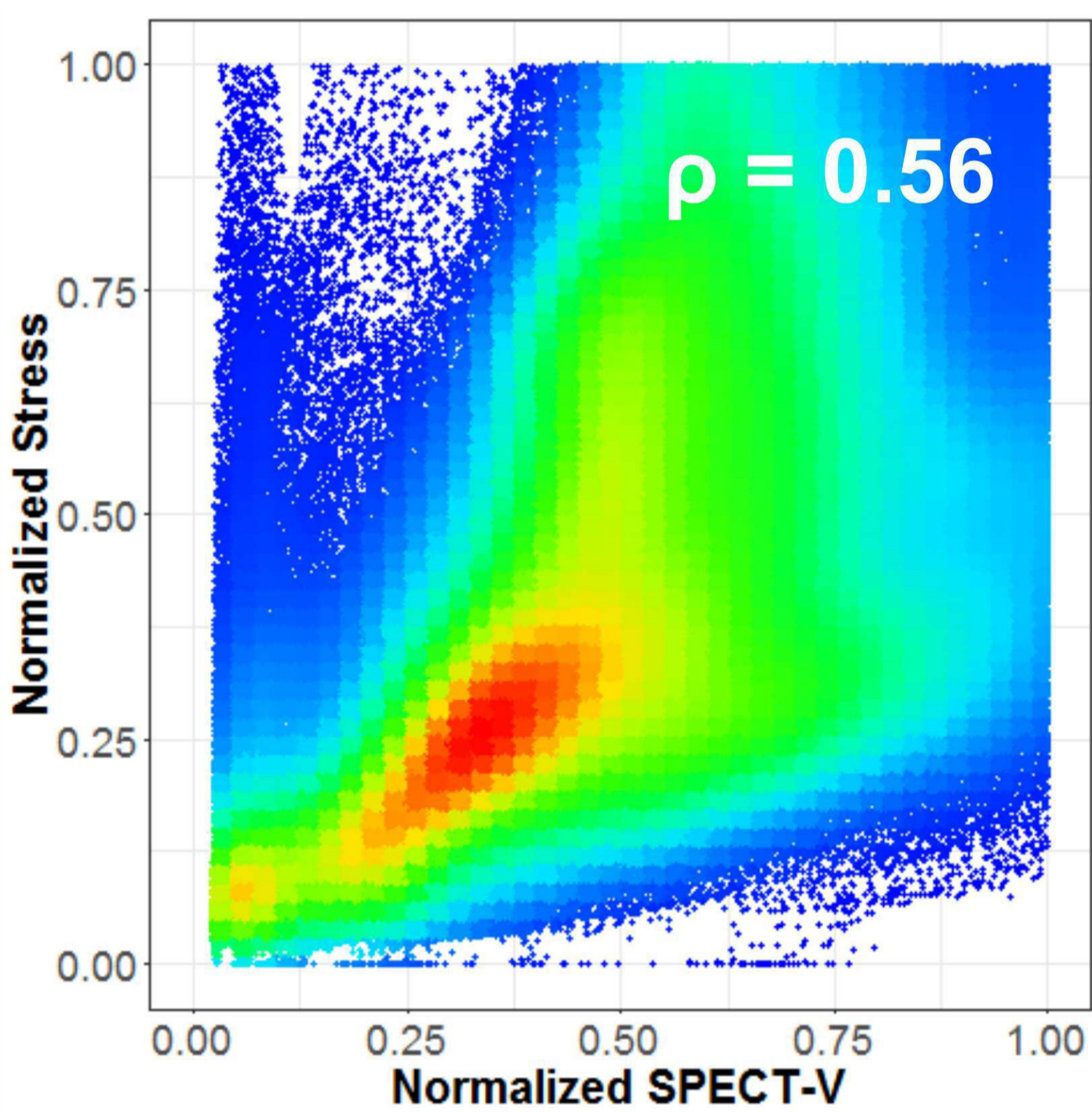
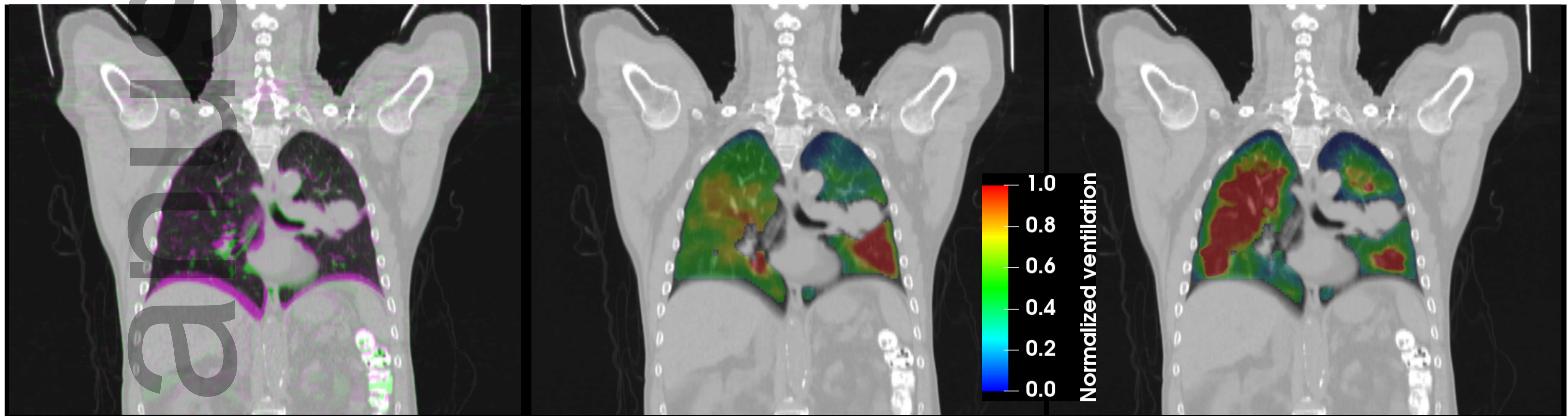
Patient 1



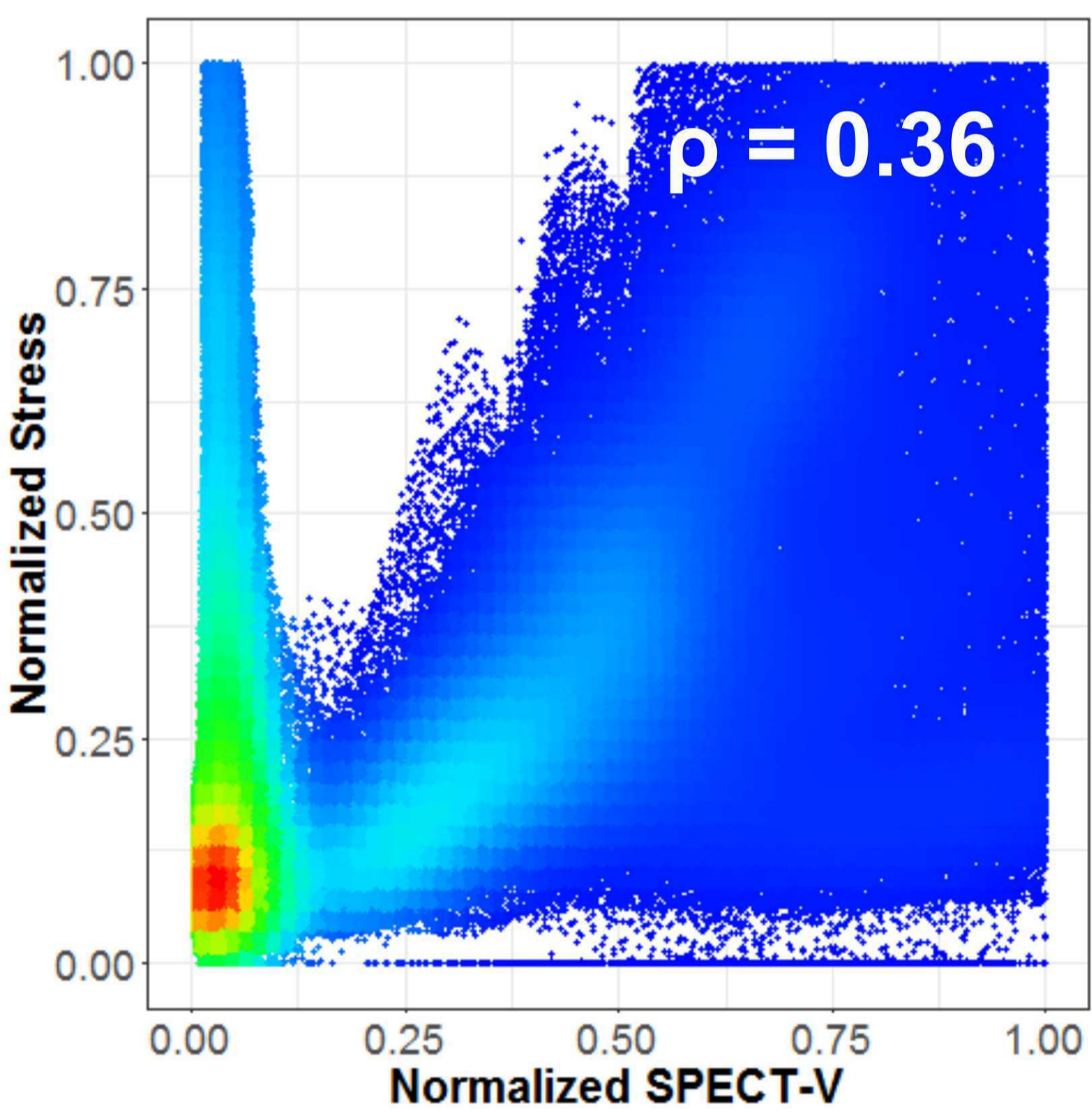
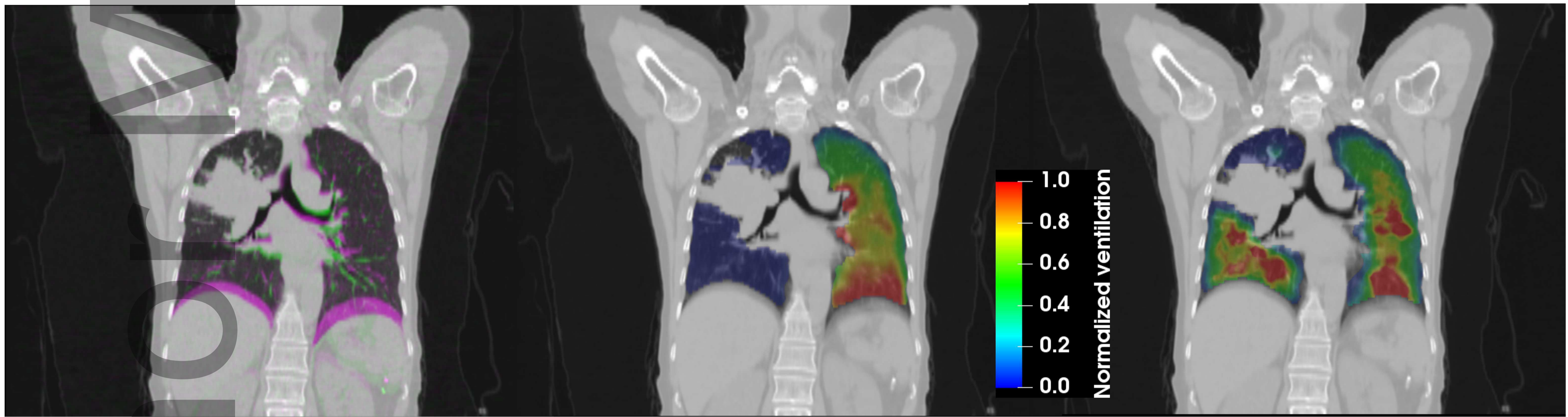
Patient 2



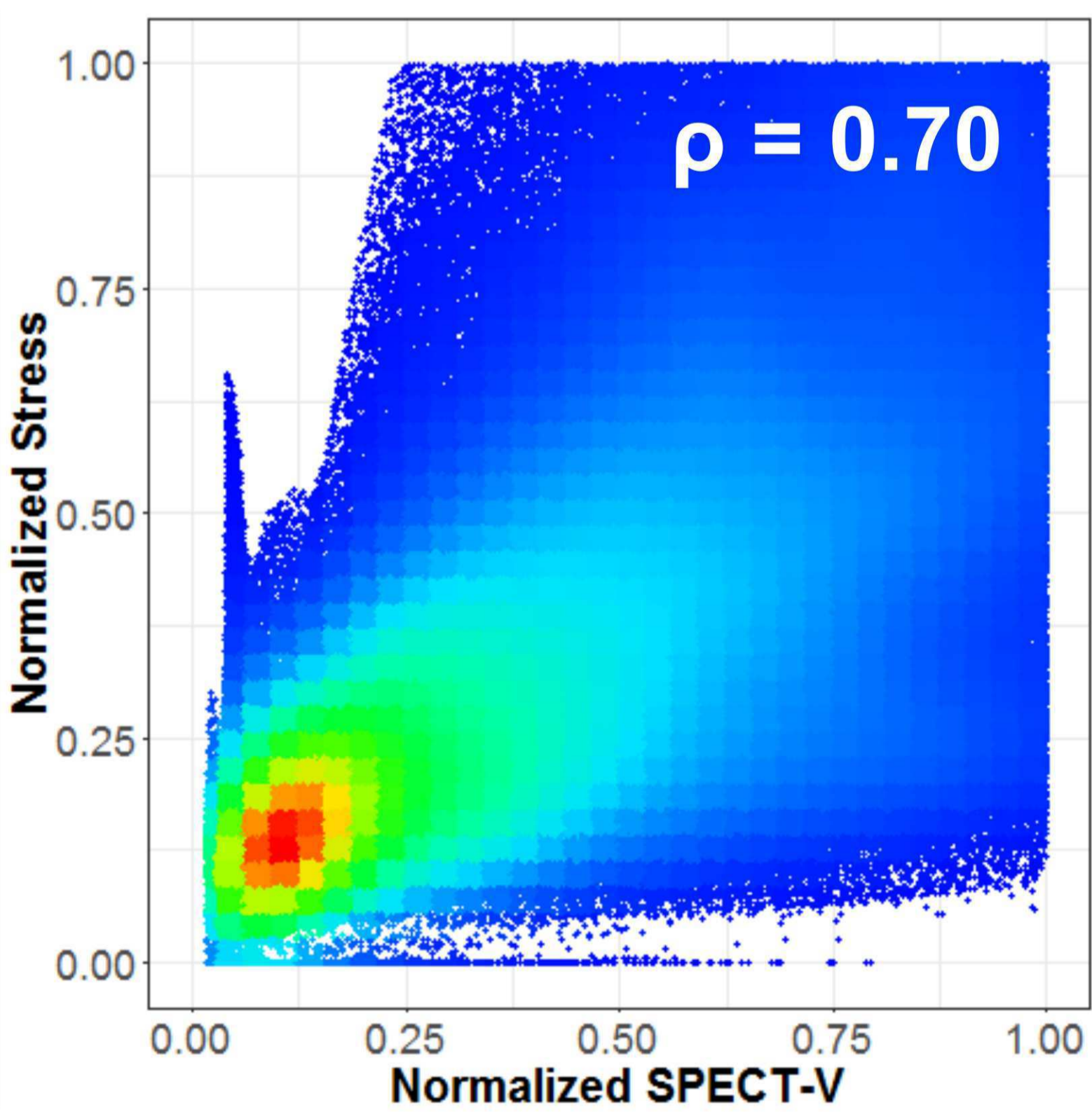
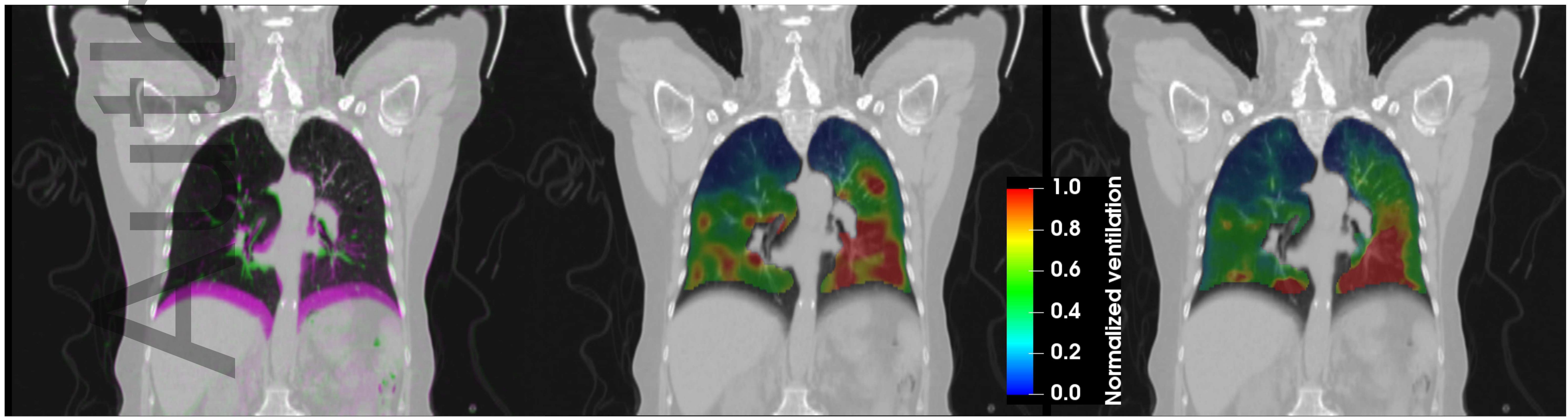
Patient 3



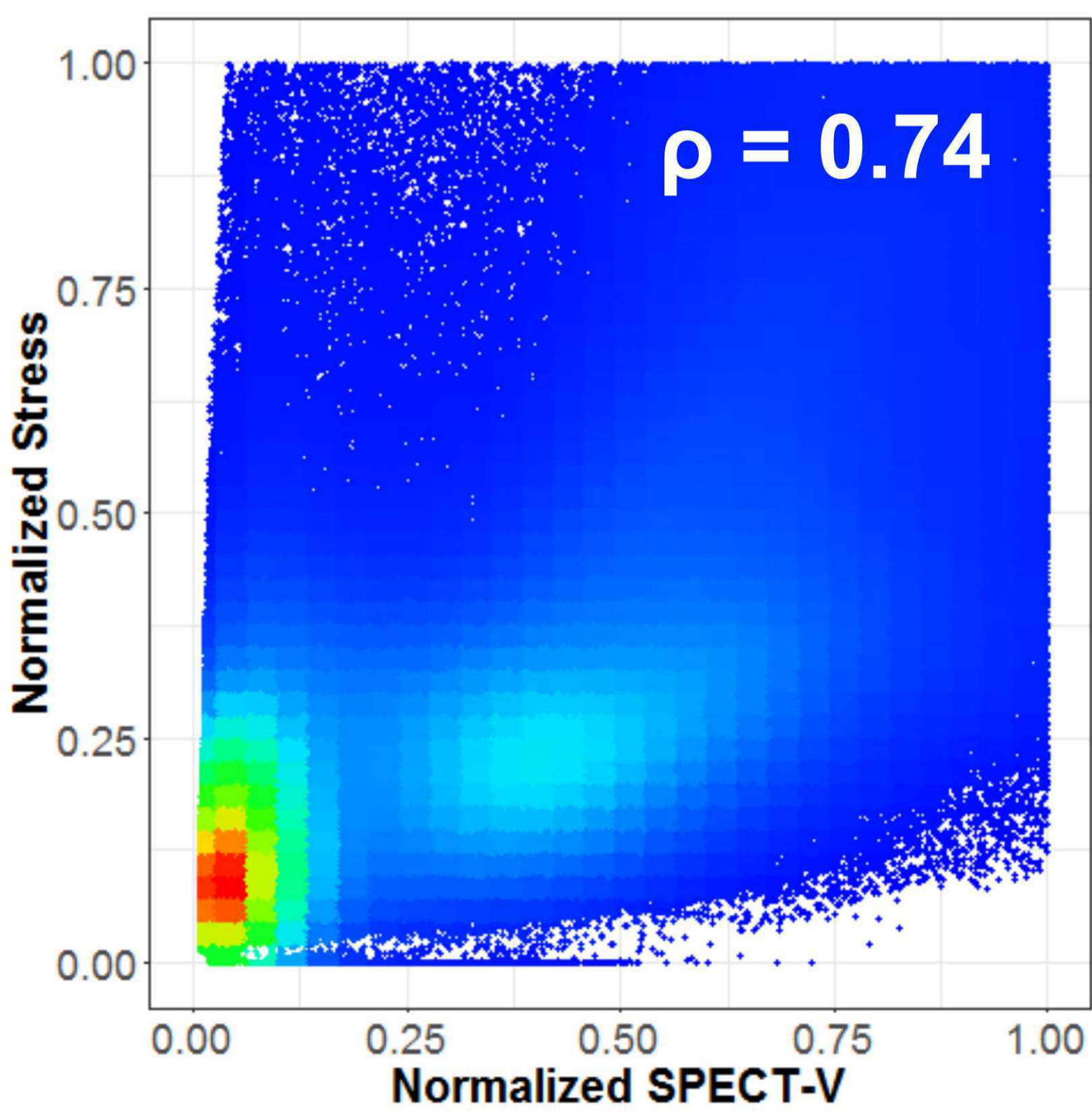
Patient 4



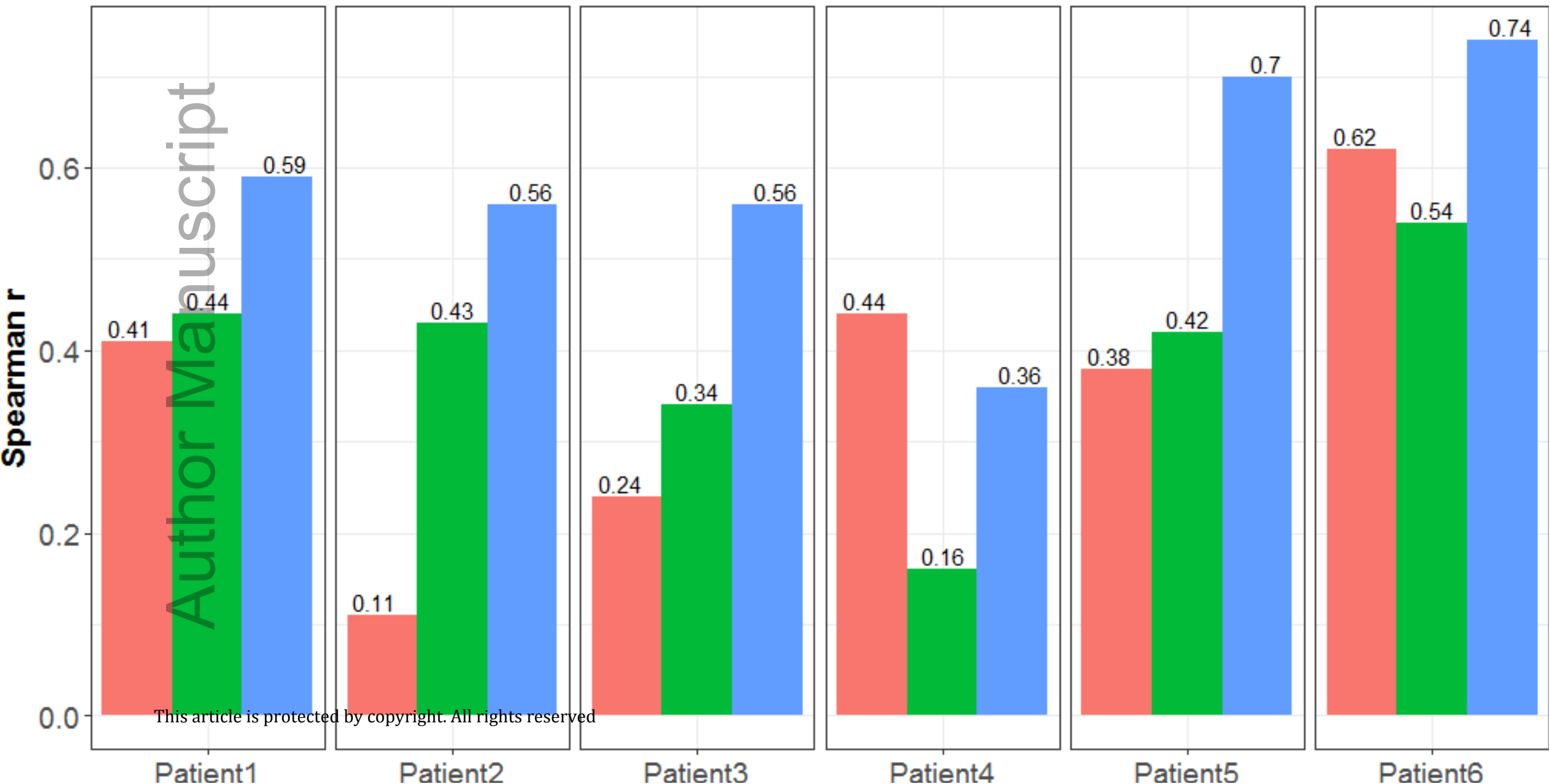
Patient 5



Patient 6



Method: ■ Hu_changes ■ Jacobian ■ Stress



Author Manuscript

This article is protected by copyright. All rights reserved

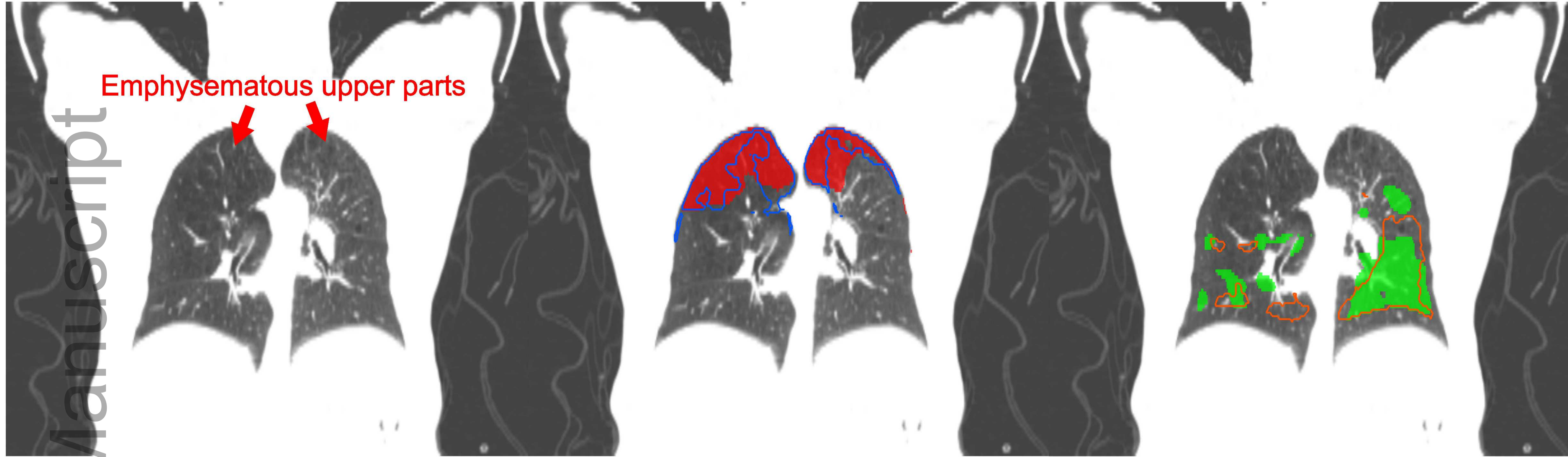
Inhale CT

**Low ventilation
function volumes**

**High ventilation
function volumes**

Patient 5

Emphysematous upper parts



Non-aerated upper lobe



Patient 6

